IOP Publishing Plasma Physics and Controlled Fusion

Plasma Phys. Control. Fusion **56** (2014) 104004 (21pp) doi:10.1088/0741-3335/56/10/104004

Nonlinear control and online optimization of the burn condition in ITER via heating, isotopic fueling and impurity injection

Mark D Boyer and Eugenio Schuster

Department of Mechanical Engineering and Mechanics, Lehigh University, Bethlehem, PA 18015, USA

E-mail: m.dan.boyer@lehigh.edu

Received 20 December 2013, revised 14 May 2014
Accepted for publication 11 June 2014
Published 27 August 2014

Abstract

The ITER tokamak, the next experimental step toward the development of nuclear fusion reactors, will explore the burning plasma regime in which the plasma temperature is sustained mostly by fusion heating. Regulation of the fusion power through modulation of fueling and external heating sources, referred to as burn control, is one of the fundamental problems in burning plasma research. Active control will be essential for achieving and maintaining desired operating points, responding to changing power demands, and ensuring stable operation. Most existing burn control efforts use either non-model-based control techniques or designs based on linearized models. These approaches must be designed for particular operating points and break down for large perturbations. In this work, we utilize a spatially averaged (zero-dimensional) nonlinear model to synthesize a multi-variable nonlinear burn control strategy that can reject large perturbations and move between operating points. The controller uses all of the available actuation techniques in tandem to ensure good performance, even if one or more of the actuators saturate. Adaptive parameter estimation is used to improve the model parameter estimates used by the feedback controller in real-time and ensure asymptotic tracking of the desired operating point. In addition, we propose the use of a model-based online optimization algorithm to drive the system to a state that minimizes a given cost function, while respecting input and state constraints. A zero-dimensional simulation study is presented to show the performance of the adaptive control scheme and the optimization scheme with a cost function weighting the fusion power and temperature tracking errors.

Keywords: burn control, nonlinear control, adaptive control

(Some figures may appear in colour only in the online journal)

1. Introduction

Precise control over the plasma density and temperature will play an important role in achieving and maintaining the high levels of performance required to make nuclear fusion reactors an economical alternative energy source. Modulation of the burn condition during ramp-up/shut-down or in response to changing power demands and disturbances is made complicated by the nonlinear and coupled dynamics of the system. For certain operating points, the nonlinear coupling can cause thermal instabilities that can either lead to quenching or a thermal excursion in which the system moves to a higher temperature operating point. During poorly controlled transients, quenches, or thermal excursions, disruptive plasma instabilities could be triggered, stopping operation and potentially causing damage to the confinement vessel. Thus, an active feedback control system that can ensure good transient performance as well as stability of the desired operating points will be an important part of a comprehensive reactor control system.

In past work, the physical and technological feasibility of various potential actuators has been studied. Prior work, including [1–3], considered modulation of the auxiliary power, modulation of the fueling rate and controlled injection of

impurities as possible actuators. While these methods can be effective approaches for burn control, each have unique drawbacks that must be considered when developing a comprehensive burn control strategy.

Burn control based on auxiliary power modulation, as studied in [4–6], is most compatible with sub-ignition operating points for which the auxiliary power can be reduced to reject thermal excursions. For devices operating with very high fusion gain Q, the amount of auxiliary heating will be quite small compared to the total plasma heating, such that modulation of auxiliary power may have a limited effect on the plasma temperature. In hybrid and steady-state scenarios, the control authority may be further constrained by the need to use some auxiliary power sources to drive plasma current.

As an alternative, control of the burn condition can be achieved through modulation of the deuterium–tritium fueling rate, as proposed in [7–11], which could enable ignited operation (or operation near the minimum auxiliary power required for current drive). The approach is potentially limited by the decay rate of the density, which can be quite slow when particle recycling rates are high. Additionally, the plasma density is nonlinearly coupled to many plasma parameters, such that changes in plasma density could lead to undesirable changes in the reactor operating scenario. The nonlinear coupling is important to consider in control design since, for certain conditions, increasing density results in a net increase in heating while for others, heating is decreased. For example, in [12], where a PID (proportional–integral–derivative) control law was used to regulate fusion power using the deuterium–tritium fueling rate, the sign of the controller gains had to be flipped when switching between thermally stable points and thermally unstable ones.

Controlled impurity injection can be used as a means to increase radiative power losses and reduce fusion heating through fuel dilution. Both effects lead to a reduction of the net plasma heating, causing a reduction in temperature. For large perturbations in initial temperature, this method can require large amounts of impurities to be injected. After the excursion is rejected, additional heating power, with a consequent reduction in the fusion gain Q, is needed to compensate the excess radiation losses until the impurities are completely removed from the reactor.

Most previous work on burn control makes use of only one of the available actuators (single-input control) at a time and studies the range of perturbations that can be rejected by the actuator. Prior work combining actuation mechanisms include [12–16] for zero-dimensional (volume-averaged) models. Studies of kinetic control and thermal stability for 1D (radial profile) models can be found in [17–19]. In [20], a diagonal multi-input, multi-output linear control scheme for burning plasma kinetics was developed by observing actuator influences during numerical simulations of plasma physics codes. The approximation of the nonlinear burning plasma model by a linearized one for controller design is a common denominator in previous model-based controller designs. The model is linearized, a controller is synthesized using linear techniques, and the resulting design is tested on the original nonlinear model. When tested in nonlinear simulations, these linear control laws succeed in stabilizing the system against a limited set of perturbations and disturbances.

In [21], a nonlinear feedback controller was synthesized that makes use of all of the previously considered actuators simultaneously. The use of nonlinear control techniques removes the limits imposed by linearization in other works and the resulting controller can accommodate very large perturbations. The controller works for suppressing both thermal excursions and quenches, can operate at sub-ignition and ignition points (or points near the minimum power required for current drive), and can drive the system from one point to another during operation. Only those works that use non-model based control techniques, like neural networks [22, 23], have also followed these guidelines. A zero-dimensional (volume-averaged) simulation study was performed to show the capabilities of the model-based controller and compare it with previous linear controllers.

Despite the advantages of the nonlinear controller designed in [21] over previous designs, the use of impurity injection could lead to undesirable accumulation of impurity ions within the plasma core, which could reduce the efficiency of the reactor long after thermal excursions are rejected. As an alternative to impurity injection, we introduced a nonlinear controller exploiting the dependence of the fusion power on the fraction of tritium in the deuterium–tritium plasma as a means of altering fusion heating [24]. Such an approach is made possible by independent control of deuterium and tritium fuel sources, a technique called isotopic fuel tailoring [25], and by the availability of diagnostics for measuring the tritium ratio in both the edge and core plasma [26–28]. By combining this technique with modulation of auxiliary heating, control of the burn condition can be maintained, even when the auxiliary power saturates, without resorting to impurity injection. While the use of isotopic fueling to control plasma heating is a promising tool for burn control, its usefulness may be limited to some extent due to particle recycling. In this process, particles lost from the plasma strike the walls of the reactor are reflected or re-emitted back to the plasma and act as a refueling source. This decreases the dependence of the tritium fraction on the controlled fuel injection, slowing response time. We include this effect through the addition of particle recycling to the model and overcome the possible limitations by utilizing impurity injection as a back-up actuator. To ensure asymptotic tracking of the target operating point despite uncertainties in the burning plasma model used for control design, the nonlinear controller is augmented with an adaptive control scheme designed to improve the model used for control design in real-time.

Though the nonlinear adaptive control scheme proposed in this work can drive the burn condition to the desired reference (defined by the energy, density and tritium fraction), the model uncertainty may lead to differences between the resulting outputs, like fusion power or divertor heat load, and those predicted by the model. For example, differences in impurity or alpha particle confinement could alter radiation losses and DT fuel content in the plasma at the reference values of E, n and γ. With large enough parameter changes, the outputs for a given reference could differ significantly from the predicted

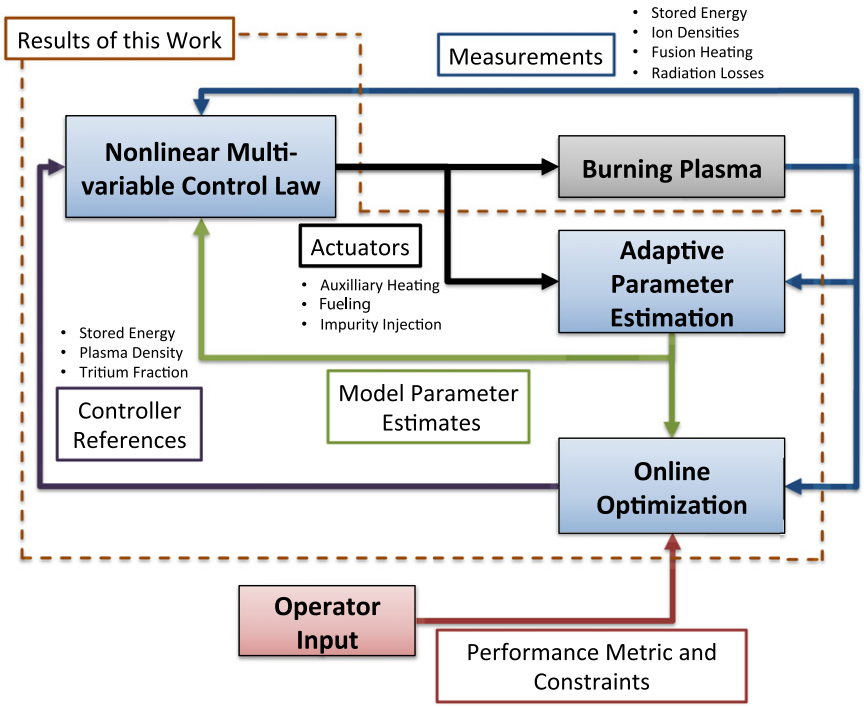

Figure 1. Schematic of proposed control scheme.

values, making it difficult to choose the controller references prior to a discharge. To overcome this issue, an online burn condition optimization scheme, inspired by the general approach proposed in [29, 30] is used to alter the controller references in real-time to minimize a cost function related to the desired reactor performance. This cost function can be chosen to weight a variety of possible outputs (either measured or predicted from models). For example, the simulation study in this work uses a cost function weighting the fusion heating, plasma temperature, and tritium fraction. The combined control scheme is illustrated in figure 1. Made up of nonlinear control laws, adaptive parameter estimation, and a real-time operating point optimizer, the scheme modifies heating, fueling, and impurity injection rates based on nonlinear combinations of measurements of the individual ion species densities, plasma stored energy, fusion reaction rate, and radiation loss power, in order to drive the system to a state (defined by stored energy, total plasma density, tritium fraction, alpha particle density, and impurity density) that optimizes a given cost function.

The paper is organized as follows. The burning plasma model and uncertain parametric form used for controller design are given in sections 2 and 3. In section 4, the adaptive nonlinear control design is presented, and in section 5 an online optimization scheme is presented. Section 6 gives the results of a simulation study of the adaptive optimization scheme. Finally, conclusions are discussed in section 7.

2. Burning plasma model

We use a zero-dimensional (volume averaged) model for a burning plasma that employs approximate energy and particle balance equations. The model considers the deuterium and tritium ion densities separately and includes an approximate global model of particle recycling for the purposes of studying the effect of recycling parameters on controller performance. The particle and energy balance equations are given by

$$\dot{n}_\alpha = -\frac{n_\alpha}{\tau_\alpha^*} + S_\alpha, \tag{1}$$

$$\dot{n}_\mathrm{D} = -\frac{n_\mathrm{D}}{\tau_\mathrm{D}} + f_\mathrm{eff} S_\mathrm{D}^\mathrm{R} - S_\alpha + S_\mathrm{D}^\mathrm{inj}, \tag{2}$$

$$\dot{n}_\mathrm{T} = -\frac{n_\mathrm{T}}{\tau_\mathrm{T}} + f_\mathrm{eff} S_\mathrm{T}^\mathrm{R} - S_\alpha + S_\mathrm{T}^\mathrm{inj}, \tag{3}$$

$$\dot{n}_\mathrm{I,c} = -\frac{n_\mathrm{I,c}}{\tau_\mathrm{I}^*} + S_\mathrm{I}^\mathrm{inj}, \tag{4}$$

$$\dot{n}_\mathrm{I,sp} = -\frac{n_\mathrm{I,sp}}{\tau_\mathrm{I}^*} + S_\mathrm{I}^\mathrm{sp}, \tag{5}$$

$$\dot{E} = -\frac{E}{\tau_\mathrm{E}} + P_\alpha - P_\mathrm{rad} + P_\mathrm{aux} + P_\mathrm{Ohm}, \tag{6}$$

where n_α, n_D, n_T, and E are the α-particle, deuterium, tritium, and energy densities, respectively. The term $n_\mathrm{I,c}$ represents the density of impurities due to controlled impurity injection, while $n_\mathrm{I,sp}$ represents the uncontrolled impurity density that arises due to sputtering from plasma facing components of the confinement vessel. The confinement times for each respective quantity are denoted as τ_α^*, τ_D, τ_T, τ_I^*, and τ_E. The particle confinement times are assumed to scale with the energy confinement time, i.e.,

$$\tau_\alpha^* = k_\alpha^* \tau_\mathrm{E}, \quad \tau_\mathrm{D} = k_\mathrm{D} \tau_\mathrm{E}, \quad \tau_\mathrm{T} = k_\mathrm{T} \tau_\mathrm{E}, \quad \tau_\mathrm{I}^* = k_\mathrm{I}^* \tau_\mathrm{E}, \tag{7}$$

where k_α^*, k_D, k_T and k_I^* are considered constants. In this work, the α-particle and impurity particle balances make use effective confinement times chosen to account for the effects

of recycling, while the confinement times for deuterium and tritium do not, as deuterium–tritium recycling is modeled separately. The source of α-particles from fusion is given by

$$S_\alpha = \gamma\,(1-\gamma)\,n_{\rm DT}^2\langle\sigma v\rangle, \tag{8}$$

$$n_{\rm DT} = n_{\rm D} + n_{\rm T}, \tag{9}$$

$$\gamma = \frac{n_{\rm T}}{n_{\rm DT}}, \tag{10}$$

where $n_{\rm DT}$ is the density of deuterium–tritium fuel and γ is the tritium fraction. The DT reactivity $\langle\sigma v\rangle$ is a highly nonlinear, positive and bounded function of the plasma temperature, T, and is calculated by

$$\langle\sigma v\rangle = \exp\left(\frac{a}{T^{\rm r}} + a_2 + a_3 T + a_4 T^2 + a_5 T^3 + a_6 T^4\right), \tag{11}$$

where the parameters $a_{\rm i}$ and r are taken from [31].

The terms $S_{\rm D}^{\rm inj}$ and $S_{\rm T}^{\rm inj}$ (controller inputs) are the deuterium and tritium injection rates, respectively and the terms $S_{\rm D}^{\rm R}$ and $S_{\rm T}^{\rm R}$ represent the fluxes due to particle recycling, which fuel the plasma with an efficiency $f_{\rm eff}$ (typically $0.1 \leqslant f_{\rm eff} \leqslant 0.5$). The model of deuterium and tritium recycling used here is based on the following description. Upon leaving the plasma and reaching the vessel walls, a fraction $f_{\rm ref}$ (typically $0.2 \leqslant f_{\rm ref} \leqslant 0.9$) of the exiting particles may be reflected back toward the plasma, while the remainder are either absorbed by the wall material (an effect called wall pumping), or removed from the vessel by the active pumping system. The wall pumping effect causes the development of a inventory of particles in the wall, which is, over time, re-emitted back to the confinement vessel (a small percentage of particles may be trapped more permanently through processes like codeposition [32]). To avoid the need for a complex model of wall conditions and active pumping efficiency, the amount of recycling from the plasma facing surfaces can be characterized by a global recycling coefficient $R^{\rm eff} = S^{\rm R}/S^{\rm S}$ (typically $R^{\rm eff} > 0.6$), where $S^{\rm R}$ is the recycled particle flux and $S^{\rm S}$ is the particle flux to the plasma facing surfaces. The wall inventory, and consequently the re-emitted particles, will have some tritium fraction, which we denote $\gamma^{\rm PFC}$, where PFC refers to plasma facing components. The recycled (reflected or re-emitted) particles go on to fuel the plasma core with some efficiency, $f_{\rm eff}$, depending on their energy and interaction with the plasma boundary. The fraction of particles that is 'screened' by the boundary returns to the plasma facing surface again to be either reflected, absorbed, or pumped out [33]. Based on this description (see appendix A), we can derive the following expressions for the recycled flux of deuterium and tritium:

$$S_{\rm D}^{\rm R} = \frac{1}{1-f_{\rm ref}\,(1-f_{\rm eff})}\left\{f_{\rm ref}\frac{n_{\rm D}}{\tau_{\rm D}} + \left(1-\gamma^{\rm PFC}\right) \times\left[\frac{(1-f_{\rm ref}\,(1-f_{\rm eff}))\,R^{\rm eff}}{1-R^{\rm eff}\,(1-f_{\rm eff})} - f_{\rm ref}\right]\left(\frac{n_{\rm D}}{\tau_{\rm D}} + \frac{n_{\rm T}}{\tau_{\rm T}}\right)\right\}, \tag{12}$$

$$S_{\rm T}^{\rm R} = \frac{1}{1-f_{\rm ref}\,(1-f_{\rm eff})}\left\{f_{\rm ref}\frac{n_{\rm T}}{\tau_{\rm T}} + \gamma^{\rm PFC} \times\left[\frac{(1-f_{\rm ref}\,(1-f_{\rm eff}))\,R^{\rm eff}}{1-R^{\rm eff}\,(1-f_{\rm eff})} - f_{\rm ref}\right]\left(\frac{n_{\rm D}}{\tau_{\rm D}} + \frac{n_{\rm T}}{\tau_{\rm T}}\right)\right\}. \tag{13}$$

Table 1. ITER machine parameters [35].

Symbol	Description	Value
I	Plasma current	15.0 MA
R	Major radius	6.2 m
a	Minor radius	2.0 m
B	Magnetic field	5.3 T
κ_{95}	Elongation at 95% flux surface/separatrix	1.7
δ_{95}	Triangularity at 95% flux surface/separatrix	0.33
V	Plasma volume	837 m^3

The term $S_{\rm I}^{\rm inj}$ (controller input) is the injection of impurities that can be used to increase the controlled impurity density $n_{\rm I,c}$ to cool the plasma. We model the sputtering source as

$$S_{\rm I}^{\rm sp} = \frac{f_{\rm I}^{\rm sp} n}{\tau_{\rm I}^*} + f_{\rm I}^{\rm sp}\dot{n},$$

where $0 \leqslant f_{\rm I}^{\rm sp} \ll 1$ in order to maintain $n_{\rm I,sp} = f_{\rm I}^{\rm sp} n$ where n is the total plasma density. This simple model reflects the fact that there is typically a small uncontrolled impurity content in the plasma. To simplify the presentation of the controller design, we consider both impurity populations to have the same effective confinement time $\tau_{\rm I}^*$, and atomic number $Z_{\rm I}$. The total impurity content $n_{\rm I} = n_{\rm I,s} + n_{\rm I,c}$ is then governed by

$$\dot{n}_{\rm I} = -\frac{n_{\rm I}}{\tau_{\rm I}^*} + S_{\rm I}^{\rm inj} + S_{\rm I}^{\rm sp}. \tag{14}$$

$P_{\rm aux}$ (controller input) represents the auxiliary heating power, while $P_\alpha = Q_\alpha S_\alpha$ is the plasma heating from fusion where $Q_\alpha = 3.52$ MeV is the energy of α-particles. $P_{\rm rad}$ represents the radiative cooling losses, which are approximated by the expression for bremsstrahlung losses used in [34], i.e.,

$$P_{\rm rad} = A_{\rm brem}\left(n_{\rm D} + n_{\rm T} + 4n_\alpha + Z_{\rm I}^2 n_{\rm I}\right) n_{\rm e}\sqrt{T\,({\rm keV})}, \tag{15}$$

where $A_{\rm brem}$ is a constant and $n_{\rm e}$ is the electron density. The electron density is obtained from the neutrality condition $n_{\rm e} = n_{\rm D} + n_{\rm T} + 2n_\alpha + Z_{\rm I} n_{\rm I}$. The plasma density and temperature are

$$\begin{aligned} n &= n_\alpha + n_{\rm D} + n_{\rm T} + n_{\rm I} + n_{\rm e}, \\ &= 2n_{\rm D} + 2n_{\rm T} + 3n_\alpha + (Z_{\rm I}+1)\,n_{\rm I}, \end{aligned} \tag{16}$$

$$T = \frac{2}{3}\frac{E}{n}. \tag{17}$$

We approximate the Ohmic heating $P_{\rm Ohm}$ with the expression

$$P_{\rm Ohm} = 2.8\times10^{-9}\frac{Z_{\rm eff} I^2}{a^4 T^{3/2}}, \tag{18}$$

where I is in Amps and T is in keV [34].

The state-dependent energy confinement time is given by

$$\tau_{\rm E} = 0.0562 H_{\rm H} I_{\rm p}^{0.93} B_{\rm T}^{0.15} P^{-0.69} n_{\rm e19}^{0.41} M^{0.19} R^{1.97} \epsilon^{0.58} \kappa_{95}^{0.78}, \tag{19}$$

where $H_{\rm H}$ is a scalar representing uncertainty in the scaling, $I_{\rm p}$ is the plasma current (MA), $B_{\rm T}$ is the toroidal magnetic field (T), $P = P_{\rm aux} + P_{\rm Ohm} + P_\alpha - P_{\rm rad}$ is the total power (MW), $n_{\rm e19}$ is the electron density (10^{19} m^{-3}), M is the effective mass of the plasma (amu), R is the major radius (m), $\epsilon = a/R$ with a the minor radius (m), and κ_{95} is the elongation at the 95% flux

surface/separatrix [35]. We utilize the main plasma parameters and dimensions given in [35] and shown in table 1.

For the purposes of control design, we will consider the states of the burning plasma system to be n_α, n_I, E, γ, and n. This choice of state vector was found to be helpful in analyzing stability and steady-state behavior of the system, since the steady-state behavior of the presented model can be determined by a reference for the controllable states $r = [E^r, n^r, \gamma^r]^T$. The dynamic equations for n_α, n_I, and E have already been given in (1), (4), and (6), while, by noting (9), (10), and (16), the remaining two equations can be written as

$$\begin{aligned}\dot{\gamma} = & -\frac{\gamma}{\tau_\mathrm{T}} + \frac{\gamma\,(1-\gamma)}{\tau_\mathrm{D}} + \frac{\gamma^2}{\tau_\mathrm{T}} \\ & + \frac{2}{n - 3n_\alpha - (Z_\mathrm{I}+1)\,n_\mathrm{I}} \left\{ f_\mathrm{eff} S_\mathrm{T}^\mathrm{R} - S_\alpha + S_\mathrm{T}^\mathrm{inj} \right. \\ & \left. -\gamma \left[f_\mathrm{eff} \left(S_\mathrm{D}^\mathrm{R} + S_\mathrm{T}^\mathrm{R} \right) - 2S_\alpha + S_\mathrm{D}^\mathrm{inj} + S_\mathrm{T}^\mathrm{inj} \right] \right\}, \end{aligned} \tag{20}$$

$$\begin{aligned}\dot{n} = & 2 \left[-\frac{n - 3n_\alpha - (Z_\mathrm{I}+1)\,n_\mathrm{I}}{2} \left(\frac{1-\gamma}{\tau_\mathrm{D}} + \frac{\gamma}{\tau_\mathrm{T}} \right) \right. \\ & \left. + f_\mathrm{eff} \left(S_\mathrm{D}^\mathrm{R} + S_\mathrm{T}^\mathrm{R} \right) - 2S_\alpha + S_\mathrm{D}^\mathrm{inj} + S_\mathrm{T}^\mathrm{inj} \right] \\ & + 3 \left[-\frac{n_\alpha}{\tau_\alpha^*} + S_\alpha \right] + (Z_\mathrm{I}+1) \left[-\frac{n_\mathrm{I}}{\tau_\mathrm{I}^*} + S_\mathrm{I}^\mathrm{inj} + S_\mathrm{I}^\mathrm{sp} \right]. \end{aligned} \tag{21}$$

3. Uncertain parametric model

In practice, many of the parameters of the burning plasma model may be uncertain and the control algorithm must make use of estimated model parameters. In this work, we utilize an adaptive control approach to ensure reference tracking despite the model uncertainty. By defining the nonlinear transformations

$$\theta_1 = \frac{1}{k_\alpha^* H_\mathrm{H}}, \tag{22}$$

$$\theta_2 = \frac{1}{H_\mathrm{H}}, \tag{23}$$

$$\begin{aligned}\theta_3 = & \frac{1}{k_\mathrm{D} H_\mathrm{H}} - \frac{f_\mathrm{eff}}{k_\mathrm{D} H_\mathrm{H} \left[1 - f_\mathrm{ref}\,(1 - f_\mathrm{eff})\right]} \\ & \times \left\{ f_\mathrm{ref} + \left(1 - \gamma^\mathrm{PFC}\right) \left[\frac{\left(1 - f_\mathrm{ref}\,(1 - f_\mathrm{eff})\right) R^\mathrm{eff}}{1 - R^\mathrm{eff}\,(1 - f_\mathrm{eff})} - f_\mathrm{ref} \right] \right\}, \end{aligned} \tag{24}$$

$$\begin{aligned}\theta_4 = & \frac{f_\mathrm{eff} \left(1 - \gamma^\mathrm{PFC}\right)}{k_\mathrm{T} H_\mathrm{H} \left[1 - f_\mathrm{ref}\,(1 - f_\mathrm{eff})\right]} \\ & \times \left[\frac{\left(1 - f_\mathrm{ref}\,(1 - f_\mathrm{eff})\right) R^\mathrm{eff}}{1 - R^\mathrm{eff}\,(1 - f_\mathrm{eff})} - f_\mathrm{ref} \right], \end{aligned} \tag{25}$$

$$\begin{aligned}\theta_5 = & \frac{f_\mathrm{eff} \gamma^\mathrm{PFC}}{k_\mathrm{D} H_\mathrm{H} \left[1 - f_\mathrm{ref}\,(1 - f_\mathrm{eff})\right]} \\ & \times \left[\frac{\left(1 - f_\mathrm{ref}\,(1 - f_\mathrm{eff})\right) R^\mathrm{eff}}{1 - R^\mathrm{eff}\,(1 - f_\mathrm{eff})} - f_\mathrm{ref} \right], \end{aligned} \tag{26}$$

$$\begin{aligned}\theta_6 = & \frac{1}{k_\mathrm{T} H_\mathrm{H}} - \frac{f_\mathrm{eff}}{k_\mathrm{T} H_\mathrm{H} \left[1 - f_\mathrm{ref}\,(1 - f_\mathrm{eff})\right]} \\ & \times \left\{ f_\mathrm{ref} + \gamma^\mathrm{PFC} \left[\frac{\left(1 - f_\mathrm{ref}\,(1 - f_\mathrm{eff})\right) R^\mathrm{eff}}{1 - R^\mathrm{eff}\,(1 - f_\mathrm{eff})} - f_\mathrm{ref} \right] \right\}, \end{aligned} \tag{27}$$

$$\theta_7 = \frac{1}{k_\mathrm{I}^* H_\mathrm{H}}, \tag{28}$$

the model can be written as

$$\dot{n}_\alpha = -\theta_1 \frac{n_\alpha}{\tau_\mathrm{E}^\mathrm{sc}} + S_\alpha, \tag{29}$$

$$\dot{E} = -\theta_2 \frac{E}{\tau_\mathrm{E}^\mathrm{sc}} + P_\alpha - P_\mathrm{rad} + P_\mathrm{aux} + P_\mathrm{Ohm}, \tag{30}$$

$$\dot{n}_\mathrm{I} = -\theta_7 \frac{n_\mathrm{I}}{\tau_\mathrm{E}^\mathrm{sc}} + S_\mathrm{I}^\mathrm{inj} + S_\mathrm{I}^\mathrm{sp}, \tag{31}$$

$$\dot{n}_\mathrm{D} = -\theta_3 \frac{n_\mathrm{D}}{\tau_\mathrm{E}^\mathrm{sc}} + \theta_4 \frac{n_\mathrm{T}}{\tau_\mathrm{E}^\mathrm{sc}} - S_\alpha + S_\mathrm{D}^\mathrm{inj}, \tag{32}$$

$$\dot{n}_\mathrm{T} = \theta_5 \frac{n_\mathrm{D}}{\tau_\mathrm{E}^\mathrm{sc}} - \theta_6 \frac{n_\mathrm{T}}{\tau_\mathrm{E}^\mathrm{sc}} - S_\alpha + S_\mathrm{T}^\mathrm{inj}, \tag{33}$$

where $\tau_\mathrm{E}^\mathrm{sc}$ is the energy confinement time predicted by the confinement scaling expression, i.e.,

$$\tau_\mathrm{E}^\mathrm{sc} = 0.0562 I_\mathrm{p}^{0.93} B_\mathrm{T}^{0.15} P^{-0.69} n_\mathrm{e19}^{0.41} M^{0.19} R^{1.97} \epsilon^{0.58} \kappa_{95}^{0.78}.$$

Using these expressions, the equations (20) and (21) can be written in the form

$$\begin{aligned}\dot{n} = & 2 \left[(\theta_5 - \theta_3) \frac{n_\mathrm{D}}{\tau_\mathrm{E}^\mathrm{sc}} + (\theta_4 - \theta_6) \frac{n_\mathrm{T}}{\tau_\mathrm{E}^\mathrm{sc}} - 2S_\alpha + S_\mathrm{D}^\mathrm{inj} + S_\mathrm{T}^\mathrm{inj} \right] \\ & + 3 \left[-\theta_1 \frac{n_\alpha}{\tau_\mathrm{E}^\mathrm{sc}} + S_\alpha \right] + (Z_\mathrm{I}+1) \left[-\theta_7 \frac{n_\mathrm{I}}{\tau_\mathrm{E}^\mathrm{sc}} + S_\mathrm{I}^\mathrm{inj} + S_\mathrm{I}^\mathrm{sp} \right], \end{aligned} \tag{34}$$

$$\begin{aligned}\dot{\gamma} = & \frac{1}{n_\mathrm{DT}} \left\{ \theta_5 \frac{n_\mathrm{D}}{\tau_\mathrm{E}^\mathrm{sc}} - \theta_6 \frac{n_\mathrm{T}}{\tau_\mathrm{E}^\mathrm{sc}} - S_\alpha + S_\mathrm{T}^\mathrm{inj} \right. \\ & \left. -\gamma \left[(\theta_5 - \theta_3) \frac{n_\mathrm{D}}{\tau_\mathrm{E}^\mathrm{sc}} + (\theta_4 - \theta_6) \frac{n_\mathrm{T}}{\tau_\mathrm{E}^\mathrm{sc}} - 2S_\alpha + S_\mathrm{D}^\mathrm{inj} + S_\mathrm{T}^\mathrm{inj} \right] \right\}. \end{aligned} \tag{35}$$

Note that by lumping together the physical uncertain parameters through the nonlinear transformations (22)–(28), we obtain a dynamic response model (29)–(35) that is linear in the uncertain parameters $\theta = [\theta_1, \theta_2, \ldots, \theta_7]$, which simplifies the adaptive control design problem. We consider the model parameters to be bounded, i.e.,

$$\begin{aligned} & 2 \leqslant k_\alpha \leqslant 10, && 0.1 \leqslant f_\mathrm{eff} \leqslant 0.5, \\ & 2 \leqslant k_\mathrm{D} \leqslant 5, && 0.2 \leqslant f_\mathrm{ref} \leqslant 0.9, \\ & 2 \leqslant k_\mathrm{T} \leqslant 5, && 0.8 \leqslant R_\mathrm{eff} \leqslant 0.95, \\ & 2 \leqslant k_\mathrm{I} \leqslant 10, && 0.1 \leqslant \gamma^\mathrm{PFC} \leqslant 0.5, \\ & 0.75 \leqslant H_\mathrm{H} \leqslant 1.25. \end{aligned} \tag{36}$$

Note that, although the existence of bounds is necessary for the stability analysis, the control design is not dependent on the particular values of the bounds. The above bounds, though chosen to be physically relevant for devices like ITER, are only considered for the purpose of simulation. Given the constraints (36), we can determine bounds on the uncertain parameters θ, i.e.,

$$\begin{aligned} & 0.08 \leqslant \theta_1 \leqslant 0.6, && 0 \leqslant \theta_5 \leqslant 0.2647, \\ & 0.75 \leqslant \theta_2 \leqslant 1.25, && 0.0222 \leqslant \theta_6 \leqslant 0.6330, \\ & 0.0175 \leqslant \theta_3 \leqslant 0.5633, && 0.08 \leqslant \theta_7 \leqslant 0.6, \\ & 0 \leqslant \theta_4 \leqslant 0.4765. \end{aligned} \tag{37}$$

These bounds were obtained by both minimizing and maximizing each one of the nonlinear functions (22)–(28) subject to the physical constraints (36). These constrained nonlinear optimization problems were solved using an interior-point method [36, 37]. In addition to the model parameter constraints (36), θ_4 and θ_5 were restricted to being positive semi-definite to ensure that the desorbed flux from the plasma facing components, S^{PFC}, is always positive semi-definite. For the range of model parameters considered, it is always the case that $\theta_3 > \theta_5$, $\theta_6 > \theta_4$, and the eigenvalues of the matrix $\begin{bmatrix}\theta_3 & \theta_4\\ \theta_5 & \theta_6\end{bmatrix}$ are positive definite. We can exploit our knowledge of parameter bounds in our estimation strategy by projecting the estimated parameters generated by the adaptive laws onto the subspace of possible parameter values.

For the simplified model considered in this work, the reference state $r = [E^{\mathrm{r}}, n^{\mathrm{r}}, \gamma^{\mathrm{r}}]^{\mathrm{T}}$ determines the steady-state reactor parameters (fusion power, temperature, etc.). A burn control algorithm must then be designed to stabilize and track a desired reference r. We can write the dynamics of the error variables $\tilde{E} = E - E^{\mathrm{r}}$, $\tilde{n} = n - n^{\mathrm{r}}$, and $\tilde{\gamma} = \gamma - \gamma^{\mathrm{r}}$ as

$$\dot{\tilde{E}} = -\theta_2 \frac{\tilde{E}}{\tau_{\mathrm{E}}^{\mathrm{sc}}} - \theta_2 \frac{E^{\mathrm{r}}}{\tau_{\mathrm{E}}^{\mathrm{sc}}} + P_\alpha - P_{\mathrm{rad}} + P_{\mathrm{Ohm}} + P_{\mathrm{aux}} - \dot{E}^{\mathrm{r}}, \tag{38}$$

$$\dot{\tilde{\gamma}} = -\theta_6 \frac{\tilde{\gamma}}{\tau_{\mathrm{E}}^{\mathrm{sc}}} + \frac{2\left[u(\gamma^{\mathrm{r}}) + (1-\gamma)\, S_{\mathrm{T}}^{\mathrm{inj}} - \gamma S_{\mathrm{D}}^{\mathrm{inj}}\right]}{n - 3n_\alpha - (Z_{\mathrm{I}}+1)\, n_{\mathrm{I}}}, \tag{39}$$

$$\dot{\tilde{n}} = -\tilde{n}\left[-(\theta_5 - \theta_3)\frac{(1-\gamma)}{\tau_{\mathrm{E}}^{\mathrm{sc}}} - (\theta_4 - \theta_6)\frac{\gamma}{\tau_{\mathrm{E}}^{\mathrm{sc}}}\right] \tag{40}$$

$$+ v - \dot{n}^{\mathrm{r}} + 2\left(S_{\mathrm{D}}^{\mathrm{inj}} + S_{\mathrm{T}}^{\mathrm{inj}}\right), \tag{41}$$

where

$$u(\gamma^{\mathrm{r}}) = \frac{n - 3n_\alpha - (Z_{\mathrm{I}}+1)\, n_{\mathrm{I}}}{2}\left[\theta_5 \frac{(1-\gamma)}{\tau_{\mathrm{E}}^{\mathrm{sc}}} - \theta_6 \frac{\gamma^{\mathrm{r}}}{\tau_{\mathrm{E}}^{\mathrm{sc}}} - \dot{\gamma}^{\mathrm{r}} - (\theta_5 - \theta_3)\frac{\left(\gamma - \gamma^2\right)}{\tau_{\mathrm{E}}^{\mathrm{sc}}} - (\theta_4 - \theta_6)\frac{\gamma^2}{\tau_{\mathrm{E}}^{\mathrm{sc}}}\right] + (2\gamma - 1)\, S_\alpha, \tag{42}$$

$$v = \left[-n^{\mathrm{r}} + 3n_\alpha + (Z_{\mathrm{I}}+1)\, n_{\mathrm{I}}\right]\left[-(\theta_5 - \theta_3)\frac{(1-\gamma)}{\tau_{\mathrm{E}}^{\mathrm{sc}}} - (\theta_4 - \theta_6)\frac{\gamma}{\tau_{\mathrm{E}}^{\mathrm{sc}}}\right] - 4S_\alpha + 3\left[-\theta_1 \frac{n_\alpha}{\tau_{\mathrm{E}}^{\mathrm{sc}}} + S_\alpha\right] + (Z_{\mathrm{I}}+1)\left[-\theta_7 \frac{n_{\mathrm{I}}}{\tau_{\mathrm{E}}^{\mathrm{sc}}} + S_{\mathrm{I}}^{\mathrm{inj}} + S_{\mathrm{I}}^{\mathrm{sp}}\right]. \tag{43}$$

The objective of the controller designed in the following section is to ensure the stability of the origin for this dynamic system.

4. Controller design

4.1. Nominal control design

We first consider the design of a nominal controller, i.e., we assume the uncertain parameters are exactly known. In the subsequent sections, the design will be augmented to ensure stability and asymptotic tracking despite model uncertainties.

We begin the nominal controller design by looking at the energy subsystem (38). We note that $\tilde{E}$ can be driven to zero by satisfying the condition

$$f(n, E, n_\alpha, n_{\mathrm{I}}, \gamma) = -\theta_2 \frac{E^{\mathrm{r}}}{\tau_{\mathrm{E}}^{\mathrm{sc}}} + P_{\mathrm{Ohm}} + P_\alpha - P_{\mathrm{rad}} + P_{\mathrm{aux}} - \dot{E}^{\mathrm{r}} + K_{\mathrm{E}}\tilde{E} = 0. \tag{44}$$

The condition (44) can be satisfied in several different ways. The auxiliary heating term P_{aux} enters the equation directly, the actuators $S_{\mathrm{D}}^{\mathrm{inj}}$ and $S_{\mathrm{T}}^{\mathrm{inj}}$ can be used to change the α-heating term P_α by modulating the tritium fraction, and the impurity injection term $S_{\mathrm{I}}^{\mathrm{inj}}$ can be used to increase the impurity content and consequently P_{rad}. Having several methods available for controlling the energy subsystem enables us to design a control scheme that can still achieve stabilization despite saturation of one or even several of the available actuators.

Step 1. We first calculate P_{aux} as

$$P_{\mathrm{aux}}^{\mathrm{unsat}} = \theta_2 \frac{E^{\mathrm{r}}}{\tau_{\mathrm{E}}^{\mathrm{sc}}} - Q_\alpha \gamma^{\mathrm{r}}\left(1 - \gamma^{\mathrm{r}}\right) n_{\mathrm{DT}}^2 \langle\sigma v\rangle + P_{\mathrm{rad}} - P_{\mathrm{Ohm}} + \dot{E}^{\mathrm{r}} - K_{\mathrm{E}}\tilde{E}, \tag{45}$$

$$P_{\mathrm{aux}} = \mathrm{sat}\left(\frac{P_{\mathrm{aux}}^{\mathrm{unsat}} - P_{\mathrm{aux}}^{\mathrm{min}}}{P_{\mathrm{aux}}^{\mathrm{max}} - P_{\mathrm{aux}}^{\mathrm{min}}}\right)\left(P_{\mathrm{aux}}^{\mathrm{max}} - P_{\mathrm{aux}}^{\mathrm{min}}\right) + P_{\mathrm{aux}}^{\mathrm{min}}, \tag{46}$$

where $\mathrm{sat}(x) = x$ for $0 < x < 1$, 0 for $x \leqslant 0$, and 1 for $x \geqslant 1$. The limit $P_{\mathrm{aux}}^{\mathrm{max}}$ ($P_{\mathrm{aux}}^{\mathrm{max}} > P_{\mathrm{aux}}^{\mathrm{min}}$) depends on the installed power on the tokamak and the limit $P_{\mathrm{aux}}^{\mathrm{min}} \geqslant 0$ depends on the operating scenario. For example, some minimum amount of power may be needed to maintain the required amount of non-inductive current drive during a particular discharge since some sources of power (neutral beam injection, electron-cyclotron current drive, etc.) also serve as sources of plasma current.

Step 2. We next find a trajectory γ^* satisfying (44), i.e.,

$$Q_\alpha \gamma^*\left(1 - \gamma^*\right) n_{\mathrm{DT}}^2 \langle\sigma v\rangle = P_{\mathrm{rad}} - P_{\mathrm{Ohm}} - P_{\mathrm{aux}} + \theta_2 \frac{E^{\mathrm{r}}}{\tau_{\mathrm{E}}^{\mathrm{sc}}} + \dot{E}^{\mathrm{r}} - K_{\mathrm{E}}\tilde{E}. \tag{47}$$

Solving this equation yields

$$\gamma^*\left(1 - \gamma^*\right) = \frac{1}{Q_\alpha n_{\mathrm{DT}}^2 \langle\sigma v\rangle} \times \left[\theta_2 \frac{E^{\mathrm{r}}}{\tau_{\mathrm{E}}^{\mathrm{sc}}} + P_{\mathrm{rad}} - P_{\mathrm{Ohm}} - P_{\mathrm{aux}} + \dot{E}^{\mathrm{r}} - K_{\mathrm{E}}\tilde{E}\right] = C, \tag{48}$$

$$\gamma^* = \frac{1 \pm \sqrt{1 - 4C}}{2}. \tag{49}$$

Note that, if the value of P_{aux} calculated in step 1 is not saturated, then $\gamma^* = \gamma^{\mathrm{r}}$. This can be shown by substituting (45) into (47). If $0 \leqslant C \leqslant 0.25$, the two resulting solutions for γ^* are real and we take the tritium-lean solution, such that $\gamma^* \leqslant 0.5$. Since the majority of heating in burning plasmas comes from fusion, it is unlikely that C will become negative, however, a negative value of C could potentially result from choosing a very large value of the free parameter K_E. In such a case, either the value of K_E could be reduced, or the value of γ^* could be set to 0 and radiation losses could be used to cool the plasma using the approach described in step 4. If

$C \geqslant 0.25$, even the optimal isotopic mix and maximum value of auxiliary heating will not generate enough heating to satisfy $f = 0$, indicating that the requested operating point may not be achievable for the shape and plasma current parameters of the scenario (which influence energy confinement through (19)), and the amount of auxiliary heating power installed on the device. Barring this situation, based on our choice of P_{aux} and γ^*, we have that

$$f\left(n, E, n_\alpha, n_{\text{I}}, \gamma^*\right) = 0. \tag{50}$$

This allows us to write $f = \hat{\gamma}\phi_\gamma$ where $\hat{\gamma} = \gamma - \gamma^*$ and ϕ_γ is a continuous function. Noting (38), (44), we can then write the dynamics of the energy perturbation as

$$\dot{\tilde{E}} = -\theta_2 \frac{\tilde{E}}{\tau_{\text{E}}^{\text{sc}}} - K_{\text{E}}\tilde{E} + \hat{\gamma}\phi_\gamma, \tag{51}$$

and the dynamics of $\hat{\gamma}$ can be written as

$$\dot{\hat{\gamma}} = -\theta_6 \frac{\hat{\gamma}}{\tau_{\text{E}}^{\text{sc}}} + \frac{2\left[u(\gamma^*) + (1-\gamma)\, S_{\text{T}}^{\text{inj}} - \gamma S_{\text{D}}^{\text{inj}}\right]}{n - 3n_\alpha - (Z_{\text{I}}+1)\, n_{\text{I}}}. \tag{52}$$

Step 3. Having selected P_{aux} and γ^* in the previous steps, we must next choose $S_{\text{D}}^{\text{inj}}$ and $S_{\text{T}}^{\text{inj}}$ to ensure that $\tilde{E}$, $\hat{\gamma}$, and $\tilde{n}$, which are governed by (51), (52), and (41), are driven to zero. We consider the Lyapunov function $V_0 = V_n + V_{\text{E},\gamma}$ where $V_n = \frac{1}{2}\tilde{n}^2$ and $V_{\text{E},\gamma} = \frac{1}{2}k_1\tilde{E}^2 + \frac{1}{2}\hat{\gamma}^2$. It can be shown that satisfying the conditions

$$2\left(S_{\text{T}}^{\text{inj}} + S_{\text{D}}^{\text{inj}}\right) = -v - K_n\tilde{n} + \dot{n}^{\text{r}}, \tag{53}$$

$$(1-\gamma)\, S_{\text{T}}^{\text{inj}} - \gamma S_{\text{D}}^{\text{inj}} = -\frac{n - 3n_\alpha - (Z_{\text{I}}+1)\, n_{\text{I}}}{2} \times \left(k_1\tilde{E}\phi_\gamma + K_\gamma\hat{\gamma}\right) - u(\gamma^*), \tag{54}$$

where $K_n > 0$ and $K_\gamma > 0$ results in

$$\dot{V}_n = -\tilde{n}^2\left(-(\theta_5 - \theta_3)\frac{(1-\gamma)}{\tau_{\text{E}}^{\text{sc}}} - (\theta_4 - \theta_6)\frac{\gamma}{\tau_{\text{E}}^{\text{sc}}} + K_n\right) < 0, \tag{55}$$

$$\dot{V}_{\text{E},\gamma} = -k_1\theta_2\frac{\tilde{E}^2}{\tau_{\text{E}}^{\text{sc}}} - k_1K_{\text{E}}\tilde{E}^2 - \left(\frac{\theta_6}{\tau_{\text{E}}^{\text{sc}}} + K_\gamma\right)\hat{\gamma}^2 < 0, \tag{56}$$

such that $\dot{V}_0 < 0$, guaranteeing asymptotic stability of the system. The conditions (53) and (54) can be satisfied by choosing

$$S_{\text{D}}^{\text{inj}} = \frac{n - 3n_\alpha - (Z_{\text{I}}+1)\, n_{\text{I}}}{2}\left(k_1\tilde{E}\phi_\gamma + K_\gamma\hat{\gamma}\right) + u(\gamma^*) + (1-\gamma)\left(\frac{-v - K_n\tilde{n} + \dot{n}^{\text{r}}}{2}\right), \tag{57}$$

$$S_{\text{T}}^{\text{inj}} = \left(\frac{-v - K_n\tilde{n} + \dot{n}^{\text{r}}}{2}\right) - S_{\text{D}}^{\text{inj}}. \tag{58}$$

These values are subject to the constraints $0 \leqslant S_{\text{D}}^{\text{inj}} \leqslant S_{\text{D}}^{\text{inj,max}}$ and $0 \leqslant S_{\text{T}}^{\text{inj}} \leqslant S_{\text{T}}^{\text{inj,max}}$. If one of the fueling actuators saturates, we cannot satisfy both conditions of the control law, so we must choose to either control n or γ. If we choose to hold condition (54), the energy and tritium fraction subsystems will remain stable, however, the density subsystem will no longer be controlled. This could potentially lead to a violation of the density limit. To avoid this, we instead choose to maintain control of the density by satisfying (53).

Because of fueling actuator saturation, it may be possible that $\dot{V}_{\text{E},\gamma} > 0$, that is, we may not be able to ensure stability of the burn condition with the previously considered actuators. There are two possible situations to consider, either a thermal quench or an excursion. If the system is experiencing a quench, the controller has already increased auxiliary heating to its maximum, so the only alternative would be to change the magnetic plasma parameters to improve energy confinement (see (19)) or to change the reference operating point to one that is achievable. If the system is experiencing a thermal excursion, however, we can still use impurity injection to stabilize the energy subsystem, despite the heating and fueling actuator saturation. In these cases we enable the use of impurity injection by setting the flag $F_{\text{imp}} = 1$ and proceeding to step 4.

Step 4. If $F_{\text{imp}} = 1$, we use the expression for radiation losses given in (15) to find an impurity density trajectory n_{I}^* that satisfies condition (44). Defining the error $\hat{n}_{\text{I}} = n_{\text{I}} - n_{\text{I}}^*$, we can write its dynamics as

$$\dot{\hat{n}}_{\text{I}} = -\theta_7\frac{\hat{n}_{\text{I}}}{\tau_{\text{E}}^{\text{sc}}} - \theta_7\frac{n_{\text{I}}^*}{\tau_{\text{E}}^{\text{sc}}} + S_{\text{I}}^{\text{inj}} + S_{\text{I}}^{\text{sp}} - \dot{n}_{\text{I}}^*. \tag{59}$$

Based on the choice of n_{I}^*, we have that

$$f\left(n, E, n_\alpha, \gamma, n_{\text{I}}^*\right) = 0, \tag{60}$$

which allows us to write $f = \hat{n}_{\text{I}}\phi_{\text{I}}$ where ϕ_{I} is a continuous function. We can then rewrite (38) as

$$\dot{\tilde{E}} = -\theta_2\frac{\tilde{E}}{\tau_{\text{E}}^{\text{sc}}} - K_{\text{E}}\tilde{E} + \hat{n}_{\text{I}}\phi_{\text{I}}. \tag{61}$$

We take as a Lyapunov function $V_1 = V_n + V_\gamma + V_{\text{E,I}}$ where $V_\gamma = \frac{1}{2}\hat{\gamma}^2$ and $V_{\text{E,I}} = \frac{1}{2}k_3\tilde{E}^2 + \frac{1}{2}\hat{n}_{\text{I}}^2$. By satisfying

$$S_{\text{I}}^{\text{inj}} = -k_3\tilde{E}\phi_{\text{I}} + \theta_7\frac{n_{\text{I}}^*}{\tau_{\text{E}}^{\text{sc}}} - S_{\text{I}}^{\text{sp}} + \dot{n}_{\text{I}}^* - K_{\text{I}}\hat{n}_{\text{I}}, \tag{62}$$

where $K_{\text{I}} > 0$, the derivative of $V_{\text{E,I}}$ can be reduced to

$$\dot{V}_{\text{E,I}} = -k_3\theta_2\frac{\tilde{E}^2}{\tau_{\text{E}}^{\text{sc}}} - k_3K_{\text{E}}\tilde{E}^2 - K_{\text{I}}\hat{n}_{\text{I}}^2 < 0. \tag{63}$$

We modify the tritium fraction trajectory to $\gamma^* = \gamma^*_{(\text{step 2})} - K_S\int_{t_0}^{t} S_{\text{I}}^{\text{inj}}\,\text{d}t$ where $\gamma^*_{(\text{step 2})}$ is the value of γ^* calculated in step 2, $K_S > 0$, and t_0 is the time at which impurity injection was first engaged. This modification ensures that the tritium fraction is, if possible, eventually reduced to such a level that impurity injection is no longer needed, i.e., $S_{\text{I}}^{\text{inj}} \to 0$. Once $S_{\text{I}}^{\text{inj}} = 0$, we disable impurity injection in subsequent executions of the algorithm by setting $F_{\text{imp}} = 0$. By satisfying

$$2\left(S_{\text{T}}^{\text{inj}} + S_{\text{D}}^{\text{inj}}\right) = -v - K_n\tilde{n}, \tag{64}$$

$$(1-\gamma)\, S_{\text{T}}^{\text{inj}} - \gamma S_{\text{D}}^{\text{inj}} = -\frac{n - 3n_\alpha - (Z_{\text{I}}+1)\, n_{\text{I}}}{2}K_\gamma\hat{\gamma} - u(\gamma_{\text{I}}^*), \tag{65}$$

we can ensure that $\dot{V}_n < 0$, $\dot{V}_\gamma < 0$, and therefore $\dot{V}_1 < 0$, guaranteeing stability of the system. The conditions (64) and (65) can be satisfied by choosing

$$S_{\mathrm{D}}^{\mathrm{inj}} = \frac{n - 3n_\alpha - (Z_{\mathrm{I}}+1)\,n_{\mathrm{I}}}{2} K_\gamma \hat{\gamma} + u(\gamma^*) + (1-\gamma)\left(\frac{-v - K_n \tilde{n}}{2}\right), \tag{66}$$

$$S_{\mathrm{T}}^{\mathrm{inj}} = \left(\frac{-v - K_n \tilde{n}}{2}\right) - S_{\mathrm{D}}^{\mathrm{inj}}, \tag{67}$$

which are again subject to saturation. If one of the fueling actuators saturates, we again choose to hold (64) to ensure stability of the density.

4.2. ISS controller for uncertain model

Having designed a nominal controller that stabilizes the system, we now consider the effects of uncertainty in the model parameters θ. In practice, the nominal controller must utilize estimated parameters $\hat{\theta} = \theta - \tilde{\theta}$, where $\hat{\theta} = [\hat{\theta}_1, \hat{\theta}_2, \hat{\theta}_3, \hat{\theta}_4, \hat{\theta}_5, \hat{\theta}_6, \hat{\theta}_7]^{\mathrm{T}}$ and $\tilde{\theta} = [\tilde{\theta}_1, \tilde{\theta}_2, \tilde{\theta}_3, \tilde{\theta}_4, \tilde{\theta}_5, \tilde{\theta}_6, \tilde{\theta}_7]^{\mathrm{T}}$ is the estimation error. Knowing *a priori* bounds on θ allows us to restrict our estimates to within these bounds, guaranteeing that the estimation error will have a known bound. In this section, we show that the closed loop system can be rendered input-to-state-stable (ISS) [38] with respect to the estimation errors. We exploit this fact in the design of adaptive parameter estimation update laws in the next section.

We begin by considering the results of step 3. The control laws are calculated using estimated model parameters, which, when substituted into the Lyapunov functions, results in

$$\dot{V}_n = \tilde{n}^2 \left[(\theta_5 - \theta_3)\frac{(1-\gamma)}{\tau_{\mathrm{E}}^{\mathrm{sc}}} + (\theta_4 - \theta_6)\frac{\gamma}{\tau_{\mathrm{E}}^{\mathrm{sc}}} - K_n \right] + \tilde{n}\tilde{v}, \tag{68}$$

$$\dot{V}_{\mathrm{E},\gamma} = -k_1\theta_2 \frac{\tilde{E}^2}{\tau_{\mathrm{E}}^{\mathrm{sc}}} - k_1 K_{\mathrm{E}} \tilde{E}^2 - k_1 \tilde{E}\left[\tilde{\theta}_2 \frac{E^{\mathrm{r}}}{\tau_{\mathrm{E}}^{\mathrm{sc}}}\right] - \left(\frac{\theta_6}{\tau_{\mathrm{E}}^{\mathrm{sc}}} + K_\gamma\right)\hat{\gamma}^2 + \hat{\gamma}\tilde{u}, \tag{69}$$

where

$$\tilde{u} = \left[\tilde{\theta}_5 \frac{(1-\gamma)}{\tau_{\mathrm{E}}^{\mathrm{sc}}} - \tilde{\theta}_6 \frac{\gamma^{\mathrm{r}}}{\tau_{\mathrm{E}}^{\mathrm{sc}}} - \left(\tilde{\theta}_5 - \tilde{\theta}_3\right)\frac{(\gamma - \gamma^2)}{\tau_{\mathrm{E}}^{\mathrm{sc}}} - \left(\tilde{\theta}_4 - \tilde{\theta}_6\right)\frac{\gamma^2}{\tau_{\mathrm{E}}^{\mathrm{sc}}} \right] \frac{n - 3n_\alpha - (Z_{\mathrm{I}}+1)\,n_{\mathrm{I}}}{2}, \tag{70}$$

$$\tilde{v} = \left[-n^{\mathrm{r}} + 3n_\alpha + (Z_{\mathrm{I}}+1)\,n_{\mathrm{I}}\right]\left[-\left(\tilde{\theta}_5 - \tilde{\theta}_3\right)\frac{(1-\gamma)}{\tau_{\mathrm{E}}^{\mathrm{sc}}} - \left(\tilde{\theta}_4 - \tilde{\theta}_6\right)\frac{\gamma}{\tau_{\mathrm{E}}^{\mathrm{sc}}} \right] + 3\left[-\tilde{\theta}_1 \frac{n_\alpha}{\tau_{\mathrm{E}}^{\mathrm{sc}}}\right] + (Z_{\mathrm{I}}+1)\left[-\tilde{\theta}_7 \frac{n_{\mathrm{I}}}{\tau_{\mathrm{E}}^{\mathrm{sc}}}\right]. \tag{71}$$

We note that the uncertain terms are bounded, i.e.,

$$\begin{aligned} |\tilde{v}| &\leqslant 2n_{\mathrm{DT}}\left[\left|\tilde{\theta}_5 - \tilde{\theta}_3\right|\frac{(1-\gamma)}{\tau_{\mathrm{E}}^{\mathrm{sc}}} + \left|\tilde{\theta}_4 - \tilde{\theta}_6\right|\frac{\gamma}{\tau_{\mathrm{E}}^{\mathrm{sc}}}\right] + 3\left|\tilde{\theta}_1\right|\frac{n_\alpha}{\tau_{\mathrm{E}}^{\mathrm{sc}}} + (Z_{\mathrm{I}}+1)\left|\tilde{\theta}_7\right|\frac{n_{\mathrm{I}}}{\tau_{\mathrm{E}}^{\mathrm{sc}}} \\ &\quad + |\tilde{n}|\left[\left|\tilde{\theta}_5 - \tilde{\theta}_3\right|\frac{(1-\gamma)}{\tau_{\mathrm{E}}^{\mathrm{sc}}} + \left|\tilde{\theta}_4 - \tilde{\theta}_6\right|\frac{\gamma}{\tau_{\mathrm{E}}^{\mathrm{sc}}}\right] \\ &\leqslant 2\left|\tilde{\theta}_{\max}\right|\frac{n + |\tilde{n}|}{\tau_{\mathrm{E}}^{\mathrm{sc}}} \\ |\tilde{u}| &\leqslant 4|\tilde{\theta}_{\max}|\frac{n_{\mathrm{DT}}}{\tau_{\mathrm{E}}^{\mathrm{sc}}}, \end{aligned}$$

where $|\tilde{\theta}_{\max}| = \max(|\tilde{\theta}_1|, |\tilde{\theta}_5|, |\tilde{\theta}_6|, |\tilde{\theta}_4 - \tilde{\theta}_6|, |\tilde{\theta}_5 - \tilde{\theta}_3|, |\tilde{\theta}_7|)$. If we choose $K_n = C_n \frac{n+|\tilde{n}|}{\tau_{\mathrm{E}}^{\mathrm{sc}}}$, $K_{\mathrm{E}} = C_{\mathrm{E}} \frac{E^{\mathrm{r}}}{\tau_{\mathrm{E}}^{\mathrm{sc}}}$, and $K_\gamma = C_\gamma \frac{n_{\mathrm{DT}}}{\tau_{\mathrm{E}}^{\mathrm{sc}}}$ where C_n , C_{E}, and C_γ are positive constants, it can then be shown that the negative definite term $-K_n\tilde{n}^2$ is guaranteed to dominate the indefinite term $\tilde{n}\tilde{v}$ whenever

$$|\tilde{n}| \geqslant 2\frac{\left|\tilde{\theta}_{\max}\right|}{C_n}.$$

Furthermore, the indefinite terms $-k_1\tilde{E}[\tilde{\theta}_2 \frac{E^{\mathrm{r}}}{\tau_{\mathrm{E}}^{\mathrm{sc}}}]$ and $\hat{\gamma}\tilde{u}$ are dominated by $-k_1 K_{\mathrm{E}}\tilde{E}^2$ and $-K_\gamma\hat{\gamma}^2$, respectively, whenever conditions

$$\left|\tilde{E}\right| \geqslant \frac{\left|\tilde{\theta}_2\right|}{C_{\mathrm{E}}},$$

$$|\hat{\gamma}| \geqslant \frac{4\left|\tilde{\theta}_{\max}\right|}{C_\gamma},$$

are satisfied. This implies that the system is ISS with respect to the model uncertainty. A similar analysis can be completed for the results of step 4.

4.3. Adaptive parameter update laws

The use of a controller that renders the system ISS with respect to bounded uncertainties allows us to design an adaptive parameter estimation update law separately from the controller [39]. This simplifies the design and analysis, gives us freedom to choose from among the various types of adaptive laws that are available, and enables the incorporation of techniques that make the adaptive system robust to disturbances and unmodeled dynamics. In order to identify the uncertain parameters, we will construct an observer for the burning plasma system based on the estimated model parameters, and render the prediction error of this system asymptotically stable through choice of parameter update laws. We define the observer for the system as

$$\begin{aligned} \dot{n}_\alpha^{\mathrm{ob}} &= -\hat{\theta}_1\frac{n_\alpha}{\tau_{\mathrm{E}}^{\mathrm{sc}}} + S_\alpha - K_\alpha^{\mathrm{ob}}\left(n_\alpha^{\mathrm{ob}} - n_\alpha\right), \\ \dot{E}^{\mathrm{ob}} &= -\hat{\theta}_2\frac{E}{\tau_{\mathrm{E}}^{\mathrm{sc}}} + P_\alpha - P_{\mathrm{rad}} + P_{\mathrm{aux}} + P_{\mathrm{Ohm}} - K_{\mathrm{E}}^{\mathrm{ob}}\left(E^{\mathrm{ob}} - E\right), \\ \dot{n}_{\mathrm{I}}^{\mathrm{ob}} &= -\hat{\theta}_7\frac{n_{\mathrm{I}}}{\tau_{\mathrm{E}}^{\mathrm{sc}}} + S_{\mathrm{I}}^{\mathrm{inj}} + S_{\mathrm{I}}^{\mathrm{sp}} - K_{\mathrm{I}}^{\mathrm{ob}}\left(n_{\mathrm{I}}^{\mathrm{ob}} - n_{\mathrm{I}}\right), \\ \dot{n}_{\mathrm{D}}^{\mathrm{ob}} &= -\hat{\theta}_3\frac{n_{\mathrm{D}}}{\tau_{\mathrm{E}}^{\mathrm{sc}}} + \hat{\theta}_4\frac{n_{\mathrm{T}}}{\tau_{\mathrm{E}}^{\mathrm{sc}}} - S_\alpha + S_{\mathrm{D}}^{\mathrm{inj}} - K_{\mathrm{D}}^{\mathrm{ob}}\left(n_{\mathrm{D}}^{\mathrm{ob}} - n_{\mathrm{D}}\right), \\ \dot{n}_{\mathrm{T}}^{\mathrm{ob}} &= \hat{\theta}_5\frac{n_{\mathrm{D}}}{\tau_{\mathrm{E}}^{\mathrm{sc}}} - \hat{\theta}_6\frac{n_{\mathrm{T}}}{\tau_{\mathrm{E}}^{\mathrm{sc}}} - S_\alpha + S_{\mathrm{T}}^{\mathrm{inj}} - K_{\mathrm{T}}^{\mathrm{ob}}\left(n_{\mathrm{T}}^{\mathrm{ob}} - n_{\mathrm{T}}\right), \end{aligned}$$

where n_α^{ob}, E^{ob}, $n_{\mathrm{I}}^{\mathrm{ob}}$, $n_{\mathrm{D}}^{\mathrm{ob}}$, and $n_{\mathrm{T}}^{\mathrm{ob}}$ are the states of the observer, $\hat{\theta}$ represents model parameter estimates, and K_α^{ob}, $K_{\mathrm{E}}^{\mathrm{ob}}$, $K_{\mathrm{I}}^{\mathrm{ob}}$,

$K_{\mathrm{D}}^{\mathrm{ob}}$, and $K_{\mathrm{T}}^{\mathrm{ob}}$ are observer gains. If we define the observer error $\tilde{n}_{\alpha}^{\mathrm{ob}} = n_{\alpha}^{\mathrm{ob}} - n_{\alpha}$, $\tilde{E}^{\mathrm{ob}} = E^{\mathrm{ob}} - E$, $\tilde{n}_{\mathrm{I}}^{\mathrm{ob}} = n_{\mathrm{I}}^{\mathrm{ob}} - n_{\mathrm{I}}$, $\tilde{n}_{\mathrm{D}}^{\mathrm{ob}} = n_{\mathrm{D}}^{\mathrm{ob}} - n_{\mathrm{D}}$, and $\tilde{n}_{\mathrm{T}}^{\mathrm{ob}} = n_{\mathrm{T}}^{\mathrm{ob}} - n_{\mathrm{T}}$, the dynamics of the error can be expressed as

$$\begin{aligned}
\dot{\tilde{n}}_{\alpha}^{\mathrm{ob}} &= -\tilde{\theta}_1 \frac{n_{\alpha}}{\tau_{\mathrm{E}}^{\mathrm{sc}}} - K_{\alpha}^{\mathrm{ob}} \tilde{n}_{\alpha}^{\mathrm{ob}},\\
\dot{\tilde{E}}^{\mathrm{ob}} &= -\tilde{\theta}_2 \frac{E}{\tau_{\mathrm{E}}^{\mathrm{sc}}} - K_{\mathrm{E}}^{\mathrm{ob}} \tilde{E}^{\mathrm{ob}},\\
\dot{\tilde{n}}_{\mathrm{I}}^{\mathrm{ob}} &= -\tilde{\theta}_7 \frac{n_{\mathrm{I}}}{\tau_{\mathrm{E}}^{\mathrm{sc}}} - K_{\mathrm{I}}^{\mathrm{ob}} \tilde{n}_{\mathrm{I}}^{\mathrm{ob}},\\
\dot{\tilde{n}}_{\mathrm{D}}^{\mathrm{ob}} &= -\tilde{\theta}_3 \frac{n_{\mathrm{D}}}{\tau_{\mathrm{E}}^{\mathrm{sc}}} + \tilde{\theta}_4 \frac{n_{\mathrm{T}}}{\tau_{\mathrm{E}}^{\mathrm{sc}}} - K_{\mathrm{D}}^{\mathrm{ob}} \tilde{n}_{\mathrm{D}}^{\mathrm{ob}},\\
\dot{\tilde{n}}_{\mathrm{T}}^{\mathrm{ob}} &= \tilde{\theta}_5 \frac{n_{\mathrm{D}}}{\tau_{\mathrm{E}}^{\mathrm{sc}}} - \tilde{\theta}_6 \frac{n_{\mathrm{T}}}{\tau_{\mathrm{E}}^{\mathrm{sc}}} - K_{\mathrm{T}}^{\mathrm{ob}} \tilde{n}_{\mathrm{T}}^{\mathrm{ob}}.
\end{aligned}$$

To study the stability of the system, we consider the Lyapunov function

$$\begin{aligned}
V^{\mathrm{ob}} = &\frac{1}{2}\left(\tilde{n}_{\alpha}^{\mathrm{ob}}\right)^2 + \frac{1}{2}\left(\tilde{E}^{\mathrm{ob}}\right)^2 + \frac{1}{2}\left(\tilde{n}_{\mathrm{I}}^{\mathrm{ob}}\right)^2\\
&+\frac{1}{2}\left(\tilde{n}_{\mathrm{D}}^{\mathrm{ob}}\right)^2 + \frac{1}{2}\left(\tilde{n}_{\mathrm{T}}^{\mathrm{ob}}\right)^2 + \frac{1}{2}\tilde{\theta}\Gamma^{-1}\tilde{\theta},
\end{aligned} \tag{72}$$

where Γ is a positive definite diagonal matrix of design parameters. The derivative of V^{ob} is calculated as

$$\begin{aligned}
\dot{V}^{\mathrm{ob}} = &-K_{\alpha}^{\mathrm{ob}}\left(\tilde{n}_{\alpha}^{\mathrm{ob}}\right)^2 - K_{\mathrm{E}}^{\mathrm{ob}}\left(E^{\mathrm{ob}}\right)^2 - K_{\mathrm{I}}^{\mathrm{ob}}\left(\tilde{n}_{\mathrm{I}}^{\mathrm{ob}}\right)^2\\
&- K_{\mathrm{D}}^{\mathrm{ob}}\left(\tilde{n}_{\mathrm{D}}^{\mathrm{ob}}\right)^2 - K_{\mathrm{T}}^{\mathrm{ob}}\left(\tilde{n}_{\mathrm{T}}^{\mathrm{ob}}\right)^2 - \tilde{\theta}_1 \tilde{n}_{\alpha}^{\mathrm{ob}} \frac{n_{\alpha}}{\tau_{\mathrm{E}}^{\mathrm{sc}}} - \tilde{\theta}_2 \tilde{E}^{\mathrm{ob}} \frac{E}{\tau_{\mathrm{E}}^{\mathrm{sc}}}\\
&- \tilde{\theta}_7 \tilde{n}_{\mathrm{I}}^{\mathrm{ob}} \frac{n_{\mathrm{I}}}{\tau_{\mathrm{E}}^{\mathrm{sc}}} - \tilde{\theta}_3 \tilde{n}_{\mathrm{D}}^{\mathrm{ob}} \frac{n_{\mathrm{D}}}{\tau_{\mathrm{E}}^{\mathrm{sc}}} + \tilde{\theta}_4 \tilde{n}_{\mathrm{D}}^{\mathrm{ob}} \frac{n_{\mathrm{T}}}{\tau_{\mathrm{E}}^{\mathrm{sc}}} + \tilde{\theta}_5 \tilde{n}_{\mathrm{T}}^{\mathrm{ob}} \frac{n_{\mathrm{D}}}{\tau_{\mathrm{E}}^{\mathrm{sc}}}\\
&- \tilde{\theta}_6 \tilde{n}_{\mathrm{T}}^{\mathrm{ob}} \frac{n_{\mathrm{T}}}{\tau_{\mathrm{E}}^{\mathrm{sc}}} + \tilde{\theta}\Gamma^{-1}\dot{\tilde{\theta}}.
\end{aligned}$$

We can render this expression negative definite by choosing the adaptive update laws

$$\dot{\tilde{\theta}} = \frac{1}{\tau_{\mathrm{E}}^{\mathrm{sc}}}\Gamma \begin{bmatrix} \tilde{n}_{\alpha}^{\mathrm{ob}} n_{\alpha} \\ \tilde{E}^{\mathrm{ob}} E \\ \tilde{n}_{\mathrm{D}}^{\mathrm{ob}} n_{\mathrm{D}} \\ -\tilde{n}_{\mathrm{D}}^{\mathrm{ob}} n_{\mathrm{T}} \\ -\tilde{n}_{\mathrm{T}}^{\mathrm{ob}} n_{\mathrm{D}} \\ \tilde{n}_{\mathrm{T}}^{\mathrm{ob}} n_{\mathrm{T}} \\ \tilde{n}_{\mathrm{I}}^{\mathrm{ob}} n_{\mathrm{I}} \end{bmatrix}. \tag{73}$$

Note that the design parameters in Γ affect the speed of response of the adaptive update (low values result in slow convergence, while higher values achieve faster convergence at the cost of possibly oscillatory system response).

5. Online operating point optimization

As mentioned earlier, a given reference for the controlled states $r = [E^{\mathrm{r}}, n^{\mathrm{r}}, \gamma^{\mathrm{r}}]^{\mathrm{T}}$ determines the steady-state reactor parameters. Part of the burn control problem is then the selection of r in such a way that a particular figure of merit for reactor performance is optimized. In this work, we consider a convex (at least locally) cost function $p(r, x, \hat{\theta})$ where $x = [n_{\alpha}, n_{\mathrm{I}}]^{\mathrm{T}}$. We assume the states of the system to be constrained within a region of parameter space over which the cost function is convex, guaranteeing a unique minimum.

Following an approach similar to the one used in [29, 30, 40], we take as a Lyapunov function

$$V_r = \frac{1}{2}\left(\frac{\partial p(r, x, \hat{\theta})}{\partial r}\right)^{\mathrm{T}} \frac{\partial p(r, x, \hat{\theta})}{\partial r}. \tag{74}$$

By taking the time derivative of V_r, we obtain

$$\dot{V}_r = \left(\frac{\partial p}{\partial r}\right)^{\mathrm{T}} \left[\frac{\partial^2 p}{\partial r^2}\dot{r} + \frac{\partial^2 p}{\partial r \partial x}\dot{x} + \frac{\partial^2 p}{\partial r \partial \hat{\theta}}\dot{\hat{\theta}}\right]. \tag{75}$$

We can then choose as an update law

$$\dot{r} = -\left(\frac{\partial^2 p}{\partial r^2}\right)^{-1} \left[K_{RTO}\frac{\partial p}{\partial r} + \frac{\partial^2 p}{\partial r \partial x}\dot{x} + \frac{\partial^2 p}{\partial r \partial \hat{\theta}}\dot{\hat{\theta}}\right], \tag{76}$$

where K_{RTO} is a diagonal positive definite matrix, leading to

$$\dot{V}_r \leqslant -\left(\frac{\partial p}{\partial r}\right)^{\mathrm{T}} K_{RTO}\frac{\partial p}{\partial r}. \tag{77}$$

This implies that $\frac{\partial p}{\partial r} \to 0$ and, therefore, r is driven toward the optimal x-dependent and $\hat{\theta}$-dependent set point, r^*. Note that the convexity of the cost function in the region of interest is required due to the need to invert $\frac{\partial^2 p}{\partial r^2}$ in the update law. This is a shortfall of the simple optimization scheme used here. However, the proposed nonlinear adaptive controller is independent of the optimization scheme used, and a more robust approach or a means of supervising the calculation to prevent numerical problems could be implemented in the future to relax this requirement.

5.1. Constrained optimization

It is important to include constraints in the optimization problem for several reasons. First, there are MHD stability limits that must be avoided, including the β limit and the Greenwald density limit. Violating these constraints could cause plasma disruptions and potentially damage the confinement vessel. Additionally, the optimized references should respect the physical limitations of the available actuators. If these limits are not considered, the optimization scheme may converge to a set of references that are not physically achievable and the burning plasma system will converge to a different (possibly far from optimal) operating point. By considering the limitations, the optimization scheme will converge to the optimal physically achievable reference. This approach could enable the control system to respond to actuator faults (e.g., loss of a beam) and find new optimal operating points. Finally, upper and lower bounds on the references can be included in the scheme to supervise the optimization process and prevent unreasonable references from being selected. In order to include these constraints in the optimization scheme, they are first written in the form $g_i(E, n, \gamma, n_{\alpha}, n_{\mathrm{I}}) \leqslant 0$, where $i \in \{1, \ldots, K\}$ and K is the number of constraints. For example, to constrain the stored energy below a maximum value of $E^{\max}$, the constraint

function would take the form $g = E - E^{\max} \leqslant 0$. The interior-point barrier function method to constrained optimization is used in this work, i.e., an augmented cost function is written in the form

$$p_c = p - \frac{1}{\eta_c} \sum_{i=1}^{K} \ln(-g_i). \tag{78}$$

where η_c is a free parameter that acts roughly as a tolerance, affecting how close the optimization scheme will come to violating the constraint. Note that the optimization scheme must be initialized at a feasible point (one that does not violate the constraints), but is otherwise unchanged.

6. Simulation study

6.1. Simulation of static and adaptive controllers

In this section, the results of two closed loop simulations, one with $\Gamma = 0$ (see (72) and (73)), i.e., without adaptation, and one with $\Gamma = \text{diag}(8, 2 \times 10^{16}, 0.05, 0.05, 0.05, 0.05, 8) \times 10^{-38}$, i.e., with adaptation, are compared. The simulations considered a nominal impurity content of 1×10^{18}#/m^3, and the atomic number of the impurity species was taken to be $Z_I = 6$. The confinement scaling parameters were taken to be $H_H = 1.1$, $k_\alpha^* = k_D = k_T = 3$, and $k_I^* = 10$. Because some experimental scenarios will rely on achieving a certain level of non-inductive current drive, we consider, as an example, the power of neutral beam injection (NBI) and electron-cyclotron current drive (ECCD) to be unavailable for feedback modulation by the burn control scheme. In the following, we consider the total power of these sources to be fixed at $P_{cd} = 53$ MW. We consider, once again as an example, an installed ion-cyclotron resonant heating (ICRH) power $P_{ICRH}^{\max} = 20$ MW as the available variable heating source. This makes $P_{aux}^{\min} = 53$ MW and $P_{aux}^{\max} = 73$ MW. The recycling model parameters used were $\gamma^{PFC} = 0.5$, $f_{eff} = 0.3$, $f_{ref} = 0.5$, and $R^{eff} = 0.9$. During the adaptive simulation, the parameters $K_\alpha^{ob} = K_E^{ob} = K_D^{ob} = K_T^{ob} = K_I^{ob} = 0.03$ were used. Note that both the static and adaptive controllers were initialized with the same estimates of the uncertain model parameters, i.e., $\hat{\theta}_1 = 1.3\theta_1$, $\hat{\theta}_2 = 1.3\theta_2$, $\hat{\theta}_3 = 0.7\theta_3$, $\hat{\theta}_4 = 1.3\theta_4$, $\hat{\theta}_5 = 0.7\theta_5$, $\hat{\theta}_6 = 1.3\theta_6$, and $\hat{\theta}_7 = 1.1\theta_7$.

The results of the simulations are compared in figure 2. Due to the incorrect estimates of the uncertain model parameters, the static (non-adaptive) controller resulted in a steady-state error in the energy, density, and tritium fraction, as seen in figures 2(*a*)–(*c*). By modifying the parameters estimates in real-time, the adaptive controller was able to achieve asymptotic stability of the desired equilibrium. Differences in the evolution of impurities and alpha-particles, as well as the actuator responses, are apparent in figures 2(*d*)–(*f*). The initial oscillations present during the adaptive simulation occur as the parameter estimator converges to constant estimates of the uncertain model parameters. This transient response can be adjusted through choice of the design parameters (K_α^{ob}, K_E^{ob}, K_D^{ob}, K_T^{ob}, K_I^{ob}, and Γ). The parameter estimates during the adaptive simulation are compared with their respective nominal values in figure 3. Note that, while the adaptive scheme ensures asymptotic stability of the desired operating point, it does not guarantee convergence of the model parameter estimates to their actual values unless the input signals (which are in this case determined by the feedback controller based on the reference signals E^r, n^r, and γ^r) are sufficiently exciting. We note that this is typical of adaptive control schemes and does not represent a limitation of the proposed approach. In this case, the reference signals were sufficiently exciting to cause the estimates of θ_1, θ_2, and θ_7 to converge to their nominal values.

6.2. Simulation of online optimization scheme

In this section, the results of a simulation study of the online optimization scheme are presented. The simulations use a cost function (see section 5) given by

$$p(r, x, \hat{\theta}) = \frac{w_T}{2}\left(T^r - T^p\right)^2 + \frac{w_{P_\alpha}}{2}\left(P_\alpha^r - P_\alpha^p\right)^2 + \frac{w_\gamma}{2}\left(\gamma^r - \gamma^p\right)^2 - \frac{1}{\eta_c}\sum_{i=1}^{K} \ln(-g_i(r, x, \hat{\theta})). \tag{79}$$

where T^r and P_α^r are the temperature and fusion heating evaluated at $[E^r, n^r, \gamma^r, n_\alpha, n_I]^T$. The terms T^p, P_α^p, and γ^p are targets for temperature, alpha-heating, and tritium fraction, and the tracking errors are weighted by constants w_T, w_{P_α}, and w_γ. By altering the references and weights in this general cost function, many different scenarios can be tested. The last term represents the barrier functions for constraints. The constraints considered in these simulations include

$$\begin{aligned} &n_e < f_{GW}^{\max} n_{GW}, \quad P_{ICRH} < P_{ICRH}^{\max}, \\ &\beta_N < \beta_N^{\max}, \qquad\quad P_{ICRH} > 0, \\ &\frac{E}{\tau_E} < Q_{div}^{\max}, \end{aligned}$$

where n_{GW} is the Greenwald density limit, $f_{GW} = n_e/n_{GW}$ is the Greenwald fraction, β_N is the Troyon β limit, $Q_{div}^{\max}$ is the maximum allowed heat load to the divertor. Note that the optimization approach is general and could be applied to other general cost functions.

6.2.1. Optimization scenario 1 In the following results, the controller was initialized with arbitrary references E^r and n^r, which were modified in real-time to minimize the cost function p. The reference $\gamma^r = 0.5$ was kept constant throughout this simulation, i.e., it was not modified by the real-time optimization algorithm, and w_γ was taken as zero. The other weights were taken as $w_T = 0.1$ and $w_{P_\alpha} = 1$. Constraints were not considered in the cost function. The references for fusion heating and temperature, P_α^p and T^p, which enter into the cost function, were modified twice during the simulation (at $t = 60$ s and $t = 120$ s) to show the ability of the scheme to move the system between operating points. The simulation considered a fractional content of impurities of 2%, i.e., $f_I^{sp} = 0.02$, and the atomic number of the impurity species was taken to be $Z_I = 4$. The confinement scaling parameters were taken to be $k_\alpha^* = 7$, $k_D = k_T = 3$, and $k_I^* = 10$. We again consider an installed ICRH heating power of 20 MW as the variable heating source and constant power

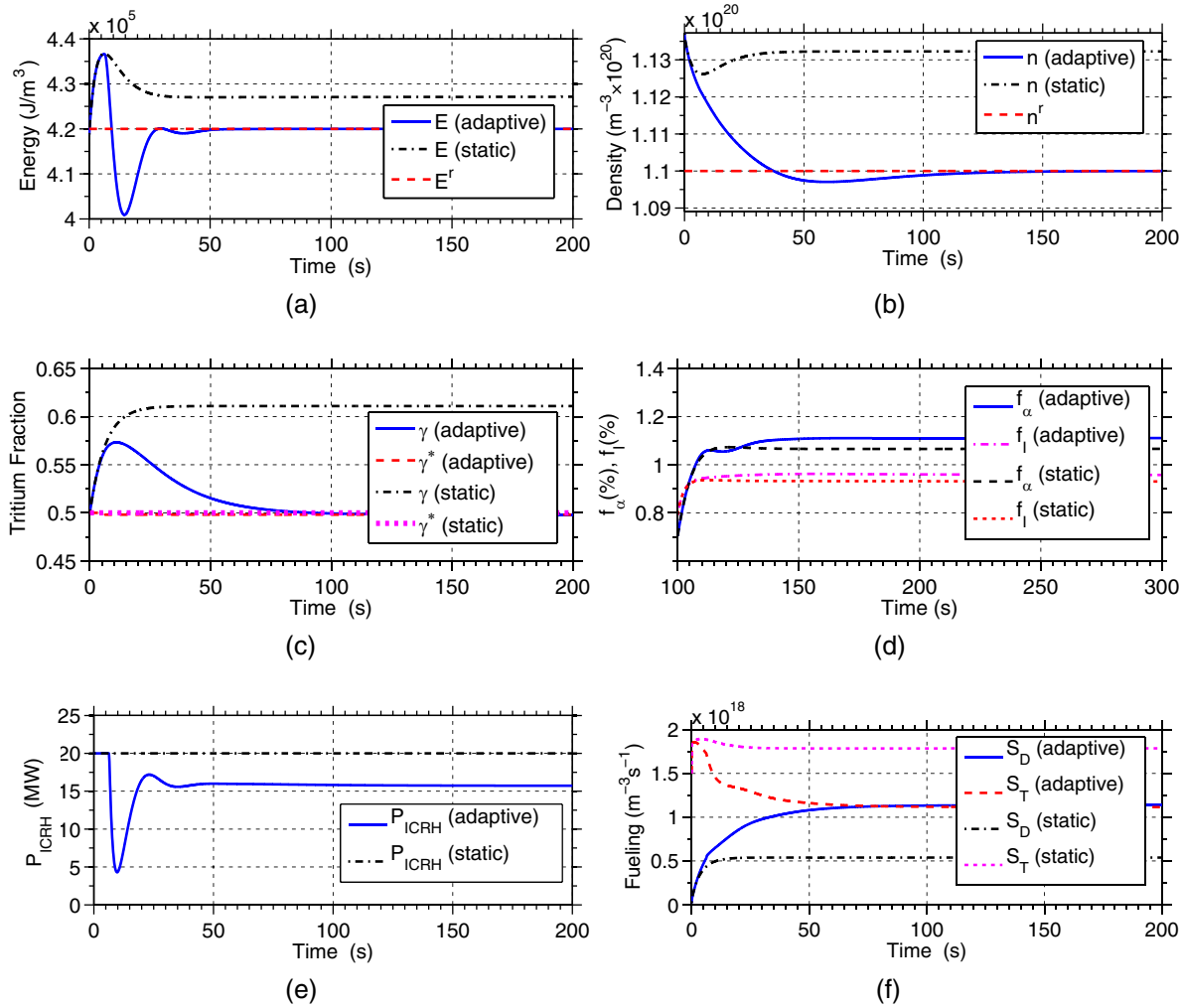

Figure 2. Comparison of states (*a*)–(*d*) and actuator trajectories (*e*) and (*f*) in static and adaptive control simulations.

of 53 MW from current drive sources, i.e., $P_{\text{aux}}^{\min} = 53\,\text{MW}$ and $P_{\text{aux}}^{\max} = 73\,\text{MW}$. The recycling model parameters used were $\gamma^{\text{PFC}} = 0.5$, $f_{\text{eff}} = 0.3$, $f_{\text{ref}} = 0.5$, and $R^{\text{eff}} = 0.95$, which represent unfavorable conditions for control of the tritium fraction. These parameters were selected to ensure that impurity injection was required during the simulation so that all aspects of the control scheme could be illustrated. Actual recycling parameters in machines like ITER may be more favorable for control such that tritium fraction control may be more effective in experiments than it is in the results shown here. A more detailed study of the effects of recycling model parameters on control performance is part of ongoing work.

The results of the simulation are shown in figure 4. The fusion heating and temperature are compared with their respective references in figures 4(*a*) and (*b*), while the system states E, n, and γ are depicted in figures 4(*c*)–(*e*). The fractional content of alpha-particles and impurities are shown in figure 4(*f*) and the actuators are given in figures 4(*g*) and (*h*). Because the initial operating point was not optimal, the optimization scheme immediately began to adjust the references E^{r} and n^{r} to move the system toward an optimal point. Due to the initial conditions of the system, a significant reduction in heating was required to track the reference E^{r} at $t = 0$, causing the auxiliary power to saturate. In order to achieve the necessary reduction in heating, the requested tritium fraction trajectory γ^* was reduced, however, the unfavorable particle recycling conditions in the simulation caused the fueling actuators to saturate and the actual tritium fraction could not track the request. To overcome this, impurity injection was enabled and used to cool the plasma. The impurity content increased for a short time until around $t = 10\,\text{s}$, at which point, due to the increasing reference E^{r}, additional auxiliary heating was required and impurity injection was disabled. The tritium fraction then returned to its reference value and the impurity content slowly decayed back to its nominal level $f_{\text{I}} = f_{\text{I}}^{\text{sp}} = 0.02$. By around $t = 40\,\text{s}$, the scheme successfully forced the system to the optimal operating point, achieving the desired fusion heating and temperature. At $t = 60\,\text{s}$ the requested fusion heating and temperature were changed and the optimization scheme adjusted the references E^{r} and n^{r} accordingly. These requests were successfully tracked by the nonlinear control scheme through a reduction in heating and fueling, and the desired fusion heating and temperature were achieved by around $t = 100\,\text{s}$. At $t = 120\,\text{s}$, the references were changed again. The reference E^{r} was

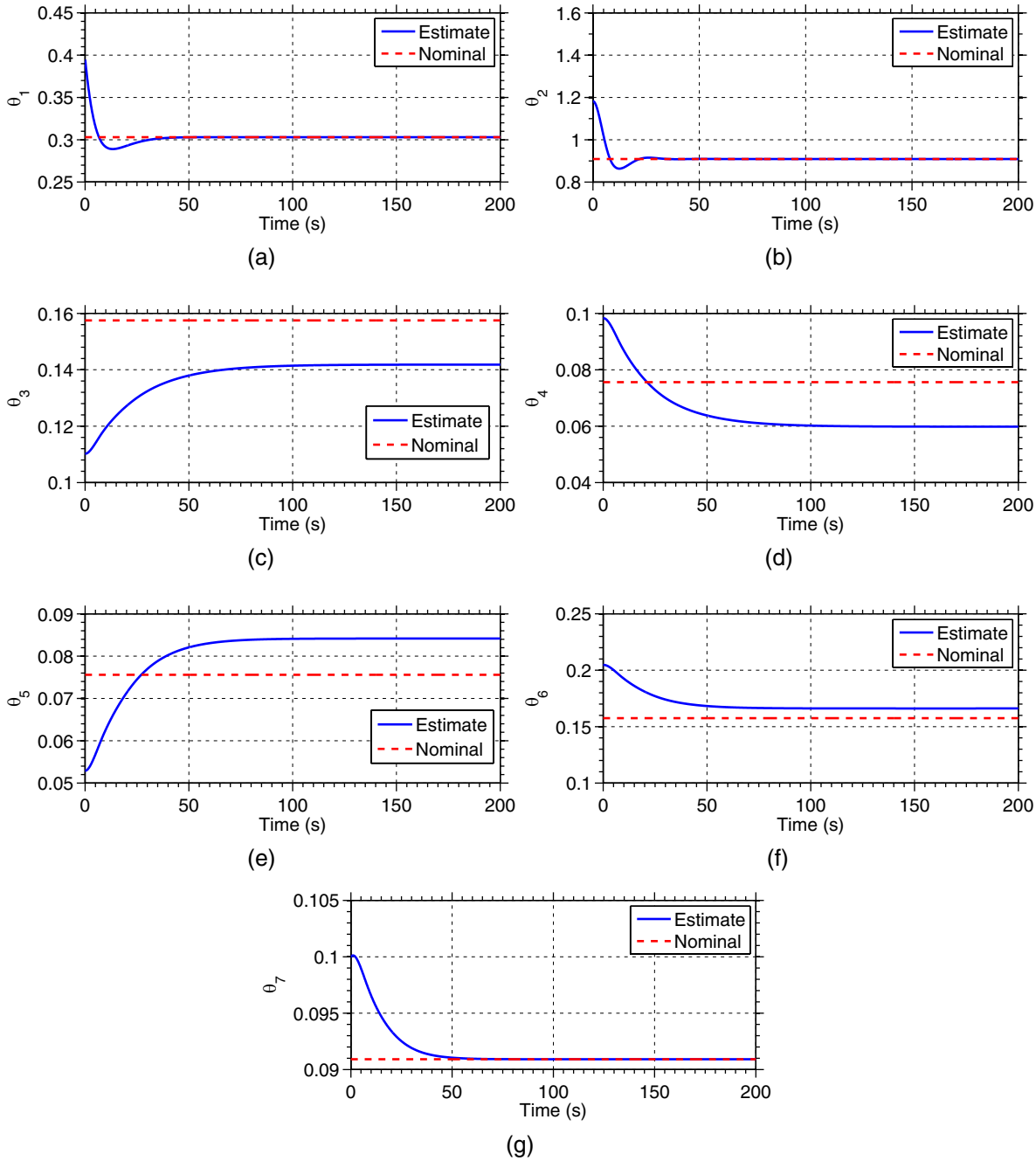

Figure 3. Comparison of estimated and nominal model parameters during the adaptive control simulation.

driven down significantly by the optimization scheme and, as a result, the auxiliary power saturated at its minimum. Again, the request γ^* was reduced and, although the actual tritium fraction began to follow the request this time, impurity injection was still needed to cool the plasma initially. By around $t = 150$ s, the tritium fraction reached the requested value γ^* and impurity injection was disabled. At about the same time, the fusion heating and temperature reached the desired values and the controller regulated the system at this operating point throughout the remainder of the simulation. Over time, the fractional content of impurities decayed back to its intrinsic level $f_I = f_I^{sp} = 0.02$ and the alpha particle content converged to its steady-state value.

6.2.2. Optimization scenario 2. In the following, the controller was initialized with arbitrary references E^r, n^r, and γ^r which were modified in real-time to minimize the cost function p (with $w_T = 0.1$, $w_{P_\alpha} = 1$, and $w_\gamma = 1$, and constraints on ICRH heating power active). This time, the cost function references for fusion heating, temperature, and tritium fraction, P_α^p, T^p, and γ^p, were kept constant throughout the simulation, however, disturbances were introduced to the system, to illustrate the controller's ability to cope with changing plasma conditions. Between $t = 250$ s and $t = 400$ s, the confinement factor H_H was ramped from 1.15 to 1.2 and held there throughout the discharge. At $t = 400$ s, the impurity content was increased by a value of 2×10^{17}#/m^3.

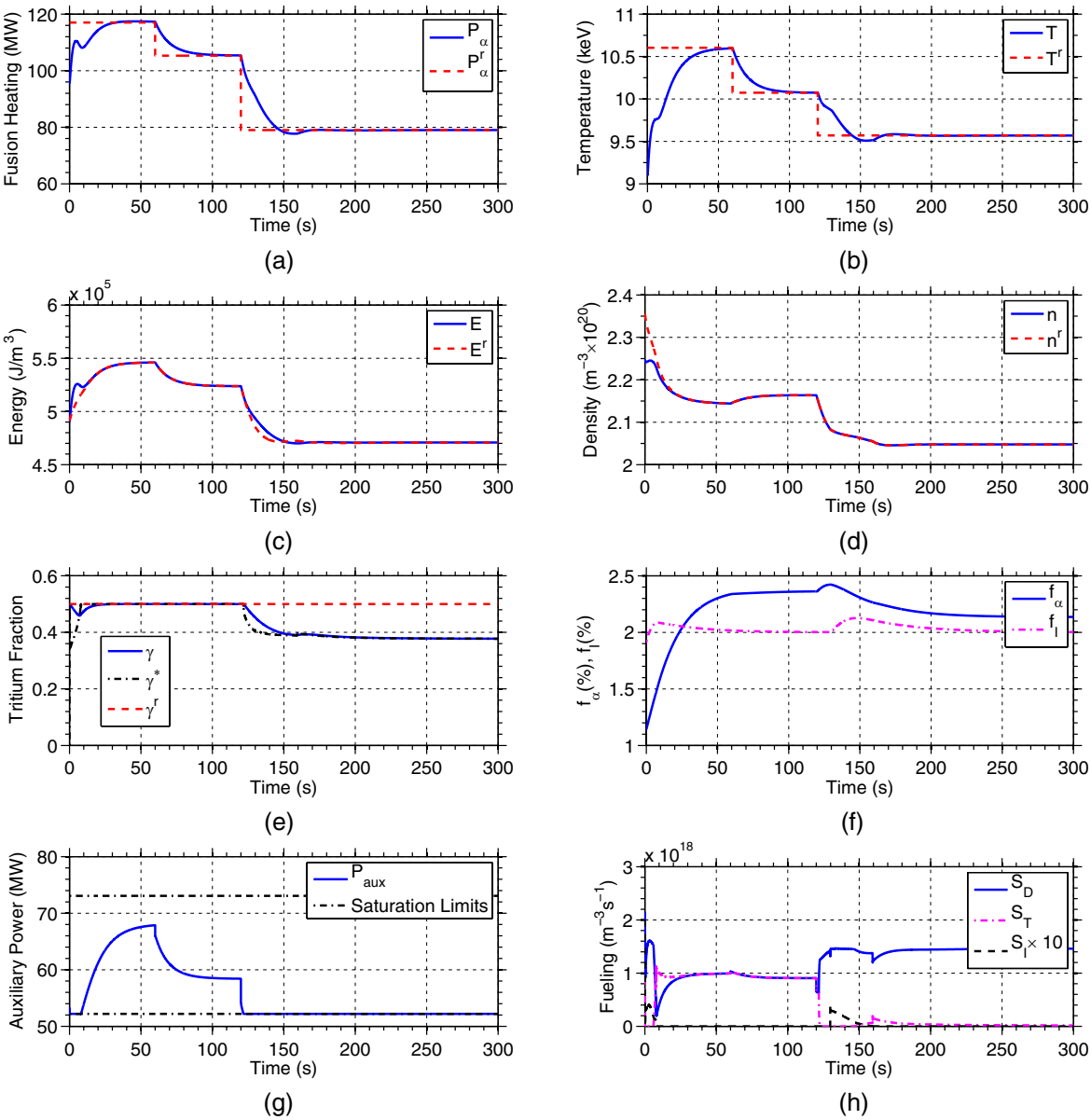

Figure 4. Closed loop evolution of (*a*) fusion heating, (*b*) temperature, (*c*) energy, (*d*) density, (*e*) tritium fraction, (*f*) alpha-fraction and impurity fraction, along with closed loop response of (*g*) auxiliary heating and (*h*) fueling actuators during the simulation of scenario 1.

The simulation considered a nominal impurity content of 1×10^{18}#/m^3, and the atomic number of the impurity species was taken to be $Z_I = 6$. The confinement scaling parameters were taken to be $k_\alpha^* = k_D = k_T = 3$, and $k_I^* = 10$. An installed ICRH power $P_{ICRH}^{max} = 20\,MW$ and a constant power from the current drive sources of $P_{cd} = 53\,MW$ was considered. The recycling model parameters $\gamma^{PFC} = 0.5$, $f_{eff} = 0.3$, $f_{ref} = 0.5$, and $R^{eff} = 0.9$ were used.

The results of the simulation are shown in figures 5 and 6. The fusion heating and temperature, the components of the cost function (79), are shown in figures 5(*a*) and (*b*), while the system states E, n, and γ are depicted in figures 5(*c*)–(*e*). The fractional content of alpha-particles and impurities are shown in figure 5(*f*) and the actuators are given in figures 5(*g*) and (*h*). Finally, the nominal and estimated model parameters are compared in figure 6. The initial operating point was again not optimal, and the optimization scheme adjusted the references E^r, n^r, and γ^r, as seen in figures 5(*c*)–(*e*), in order to reduce the cost function. Despite initial condition errors, these requests were successfully tracked by the nonlinear control scheme through modulation of the heating and fueling, and the optimal operating point, producing the desired fusion heating and temperature, was achieved by around $t = 200\,s$. At $t = 250\,s$, the confinement disturbance was ramped up, forcing the adaptive parameter estimation scheme to update its estimates, as seen in figure 6. During the transient part of the disturbance, small tracking errors can be noted in figures 5(*c*) and (*d*). The increase in confinement caused the controller to ramp down the ICRH power, eventually reaching saturation (figure 5(*g*)). The constrained online optimization scheme responded to the saturation by decreasing the reference γ^r, as seen in figure 5(*e*), resulting in an operating point that could be stabilized without ICRH heating, while still remaining close to the desired temperature and fusion power, i.e., the

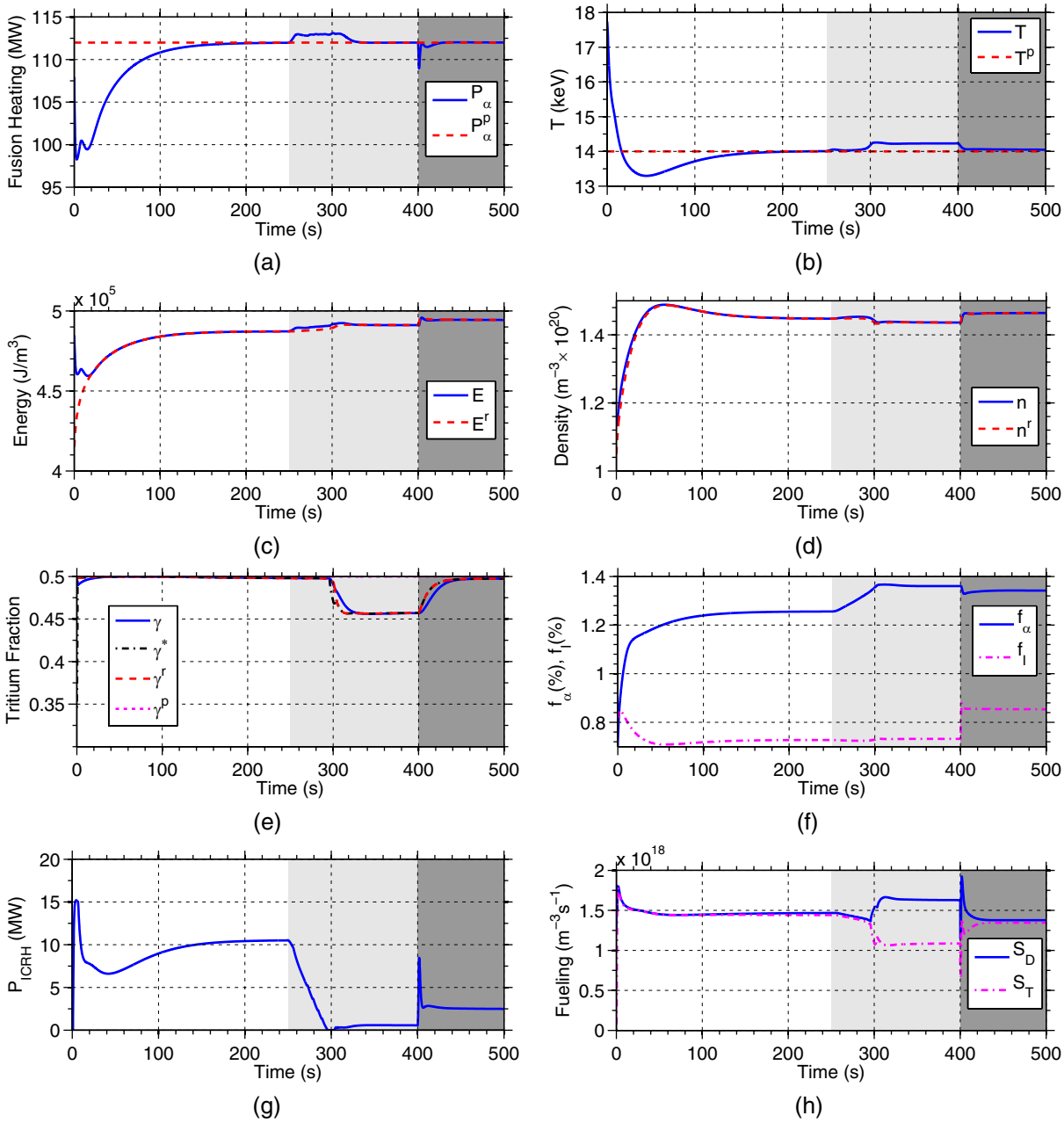

Figure 5. Closed loop evolution of (*a*) fusion heating, (*b*) temperature, (*c*) energy, (*d*) density, (*e*) tritium fraction, (*f*) alpha-fraction and impurity fraction, along with closed loop response of (*g*) auxiliary heating and (*h*) fueling actuators. The shaded light gray region indicates the time interval in which the confinement disturbance was introduced and the dark gray region indicates the impurity disturbance.

optimal feasible operating point. The desired fusion power was achieved by around $t = 320$ s, while a slight deviation from the reference temperature remained (figure 5(*b*)) due to the fact that the optimization scheme was constrained by the saturation of the ICRH power (recall that the cost function weight on fusion heating tracking error was significantly higher than that placed on the temperature tracking error). As seen in figure 5(*f*), the impurity disturbance was introduced at $t = 400$ s, which increased radiation losses and diluted the fusion fuel, causing a reduction in temperature and fusion heating. The optimization scheme responded by increasing all three controller references, and the nonlinear controller was able to track them and regulate the optimal operating point. Due to the increased impurity level, the ICRH power was increased out of saturation and the optimization scheme was able to drive the system to the optimal point, achieving the desired values P_α^{p}, T^{p}, and γ^{p}, as shown in figures 5(*c*)–(*e*). Turning to the model parameter estimates, it should be noted that only θ_2 affects the cost function (through its influence on the constrained input P_{ICRH}, which is calculated from (45)). Despite the fact that the nominal parameter changed during the simulation, the parameter estimation scheme was able to keep the estimated value close to the true value, as seen figure 6(*b*). After the confinement disturbance, the estimates of θ_3, θ_4, θ_5, and θ_6, shown in figures 6(*c*)–(*f*), do not converge to the true values, due to a lack of persistent excitation. However, this

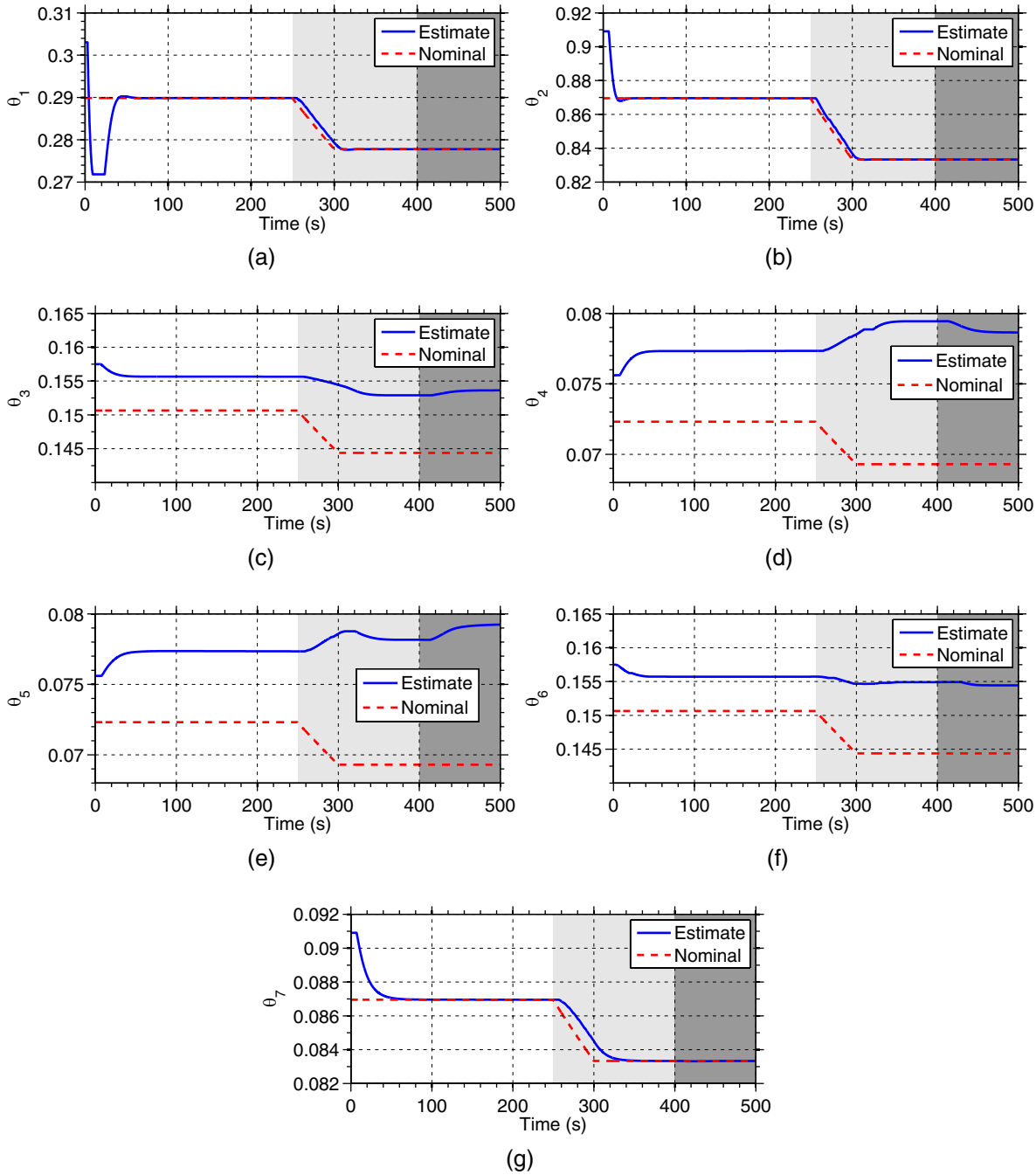

Figure 6. Comparison of estimated and nominal model parameters during the simulation of scenario 2.

does not influence the tracking performance of the control, nor does it affect the optimization scheme, as these parameters do not enter into the calculation of the cost function.

6.2.3. Optimization scenario 3 In the following, the cost function from the previous section was considered, and the references for fusion heating, temperature, and tritium fraction, $P_\alpha^{\mathrm{p}} = 120$, $T^{\mathrm{p}} = 14$, and $\gamma^{\mathrm{p}} = 0.5$, were kept constant throughout the simulation. However, this time a constraint on the divertor heat load was added, i.e., $Q_{\mathrm{div}} < Q_{\mathrm{div}}^{\max}$, where $Q_{\mathrm{div}}^{\max}$ was set to 155 MW, to illustrate the controller's ability to cope with constraints. The simulation considered a nominal impurity content of 1×10^{18}#/m^3, and the atomic number of the impurity species was taken to be $Z_{\mathrm{I}} = 6$. The confinement scaling parameters were taken to be $k_\alpha^* = k_{\mathrm{D}} = k_{\mathrm{T}} = 3$, and $k_{\mathrm{I}}^* = 10$, while the confinement factor was taken as $H_{\mathrm{H}} = 1.1$ throughout the discharge. An installed ICRH power $P_{\mathrm{ICRH}}^{\max} = 20$ MW and a constant power from the current drive sources, $P_{\mathrm{cd}} = 53$ MW, were considered. The recycling model parameters used were again $\gamma^{\mathrm{PFC}} = 0.5$, $f_{\mathrm{eff}} = 0.3$, $f_{\mathrm{ref}} = 0.5$, and $R^{\mathrm{eff}} = 0.9$.

Figure 7 compares the fusion power, temperature, heat load, and cost function during the constrained simulation with the results of an unconstrained simulation. The remaining plasma parameters during the constrained simulation are

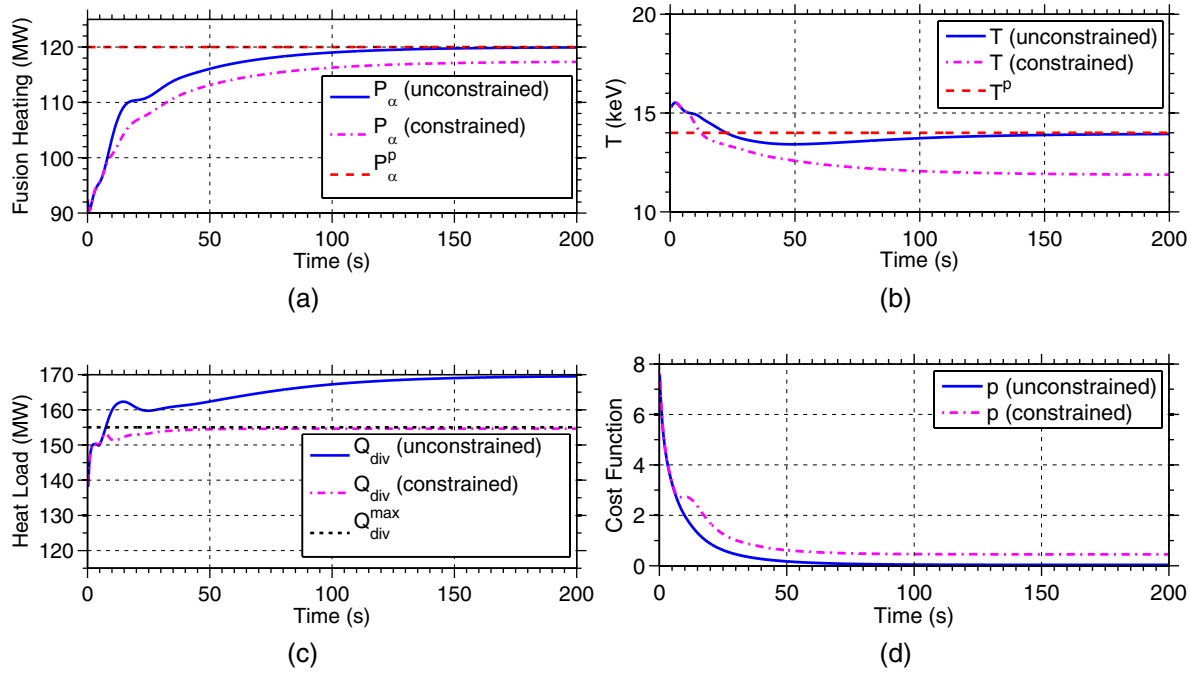

Figure 7. Comparison of (*a*) fusion heating, (*b*) temperature, (*c*) divertor heat load and (*d*) the cost function p during simulations of scenario 3 using both constrained and unconstrained optimization.

shown in figures 8 and 9. The fusion heating and temperature, the components of the cost function (79), are shown in figures 8(*a*) and (*b*), while the system states E, n, and γ are depicted in figures 8(*c*)–(*e*). The fractional content of alpha-particles and impurities are shown in figure 8(f) and the actuators are given in figures 8(g) and (h). The nominal and estimated model parameters are compared in figure 9.

Comparing the results of the constrained simulation with an unconstrained one, it can be seen that the fusion power and temperature settle to values lower than the requested ones in the constrained case, while the request values are achieved in the unconstrained case. This results in a slightly higher value of the cost function in the constrained case, as seen in figure 7(*d*). In figure 7(*c*), it can be seen that, while the unconstrained optimization scheme violates the divertor heat load constraint, the constrained version keeps the heat load below the specified limit by driving the system to the optimal feasible point. As seen in figures 8(*c*)–(*e*), the optimization scheme adjusted the references E^{r}, n^{r}, and γ^{r} to achieve the optimal operating point. Reference tracking errors can been seen decaying away in the first 50 s as the parameter estimations, shown in figure 9, converged toward a constant set of model parameter estimates.

6.2.4. Optimization scenario 4. In the following, a scenario designed to demonstrate the effect of the constraints on the Greenwald fraction (f_{GW}), β_{N}, and $P_{\mathrm{ICRH}}^{\max}$ is presented. The cost function from the previous section was considered, and the references for temperature and tritium fraction, $T^{\mathrm{p}} = 14$ and $\gamma^{\mathrm{p}} = 0.5$, were kept constant throughout the simulation. Between $t = 200$ s and $t = 250$ s, the reference for fusion heating was ramped from $P_\alpha^{\mathrm{p}} = 120$ MW to $P_\alpha^{\mathrm{p}} = 128$ MW. The confinement factor was degraded from $H_H = 1.15$ to $H_H = 1.12$ between $t = 350$ s and $t = 400$ s. The real-time optimization scheme was constrained to keep $f_{\mathrm{GW}} < 0.8$ and $\beta_{\mathrm{N}} < 3.5$, but the heat load constraint considered in the previous was not activated so the effect of the other constraints could be shown. All other parameters matched those used in scenario 3.

Figures 10(*a*)–(f) show the fusion heating, temperature, energy, density, β_{N}, and f_{GW} during the simulation, respectively. The light grey shaded region indicates the time interval in which the fusion power request is increased, while the dark grey shaded region indicates the time interval in which the confinement disturbance is introduced. It is evident that the initial reference values E^r and n^r were not optimal, and the optimization scheme begins to drive them toward values that improve tracking of the desired fusion heating and temperature from the start of the simulation. However, at around $t = 50$ s, the optimization scheme stops increasing the density reference because any further increase would violate the limit on the Greenwald fraction. Due to this constraint, the desired fusion heating and temperature are not achieved, although, because it was weighted heavier than temperature, the fusion heating is still driven quite close to the requested value. At $t = 200$ s, the request for fusion heating is increased. While the density reference is not changed due to the limit on the Greenwald fraction, the energy reference is increased to increase fusion heating. This continues until around $t = 270$ s, at which point any further increase would violate the limit placed on β_{N}. Throughout the simulation, the tritium fraction, shown in figure 10(g), remains close to 0.5, while the fractions of impurities and α particles, shown in 10(h), change slightly in response to changes in total density and fusion reaction rate. The feedback response of the actuators is depicted in figures 10(i) and 10(j). Note that, as the confinement degradation disturbance is introduced at $t = 350$s, P_{ICRH} is increased to its maximum. Since the tritium fraction is already

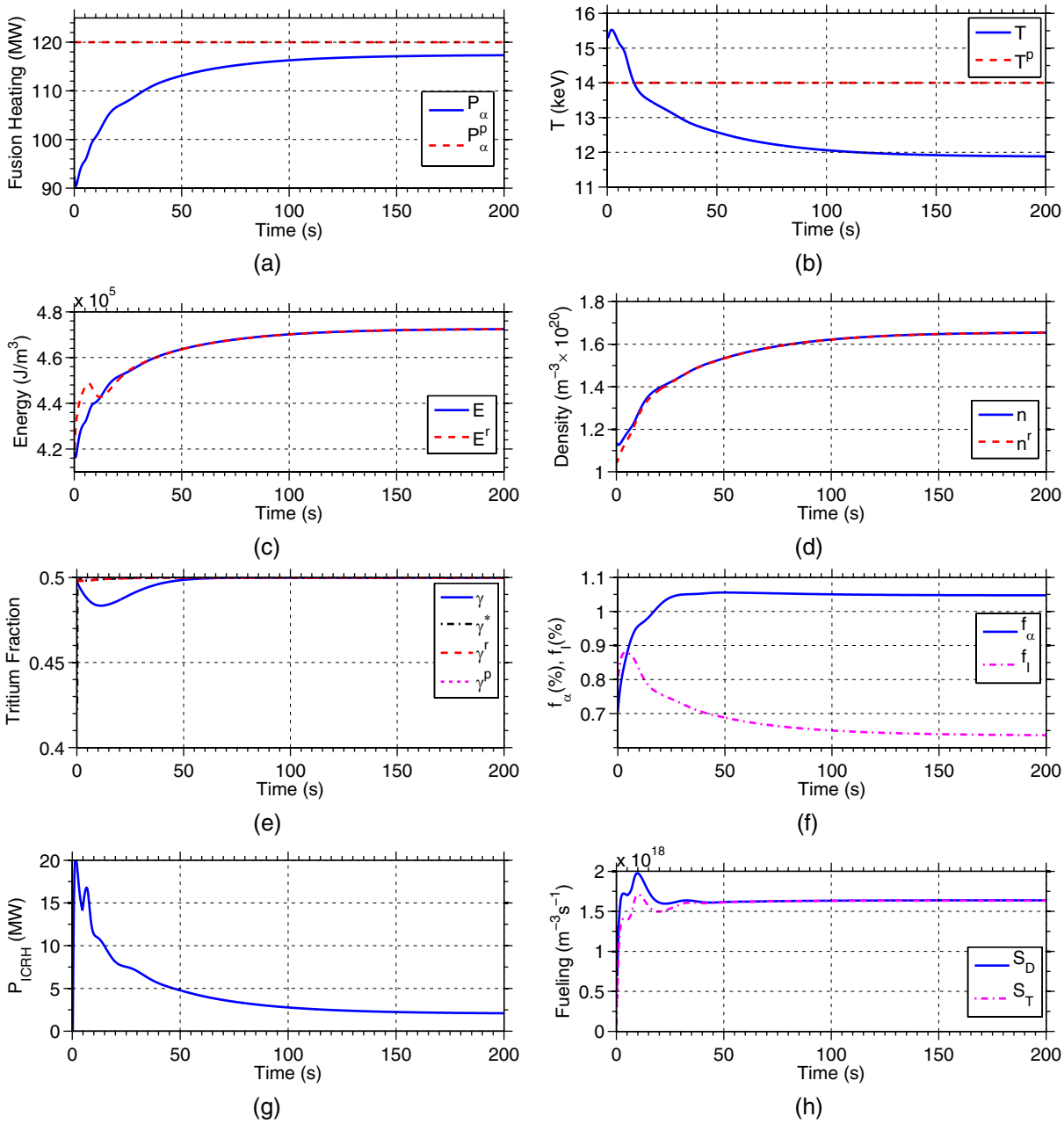

Figure 8. Closed loop evolution of (*a*) fusion heating, (*b*) temperature, (*c*) energy, (*d*) density, (*e*) tritium fraction, (*f*) alpha-fraction and impurity fraction, along with closed loop response of (*g*) auxiliary heating and (*h*) fueling actuators during the simulation of scenario 3 (constrained case).

at its maximum, the control has no further means of heating the plasma, and the energy deviates from its reference, as seen in figure 10(*c*). To ensure optimal performance, the E^r is reduced to an achievable level by an anti-windup augmentation described in appendix B. Note that the adaptive parameter estimation scheme was active during the simulation, however, because the estimates behaved in very similar ways to the previous scenarios, they are not shown here.

7. Conclusions

We have presented a nonlinear model of a burning tokamak plasma that includes a simplified model of the effects of particle recycling on density and tritium fraction dynamics. A nonlinear adaptive controller was proposed, along with a real-time model-based scheme for optimizing the operating point. The nonlinear controller combines modulation of the auxiliary power and fueling sources with impurity injection to ensure performance and stability even when one or more actuators saturate. Zero-dimensional simulations illustrate the performance of the closed loop system when moving between operating points, responding to disturbances, and dealing with constraints. Ongoing work includes studying the effect of different recycling model parameters on the performance of the control strategy, and the design of nonlinear observers to estimate states that may not be measurable in the harsh environment of a reactor [41]. In future work, a Monte Carlo simulation study will be used to systematically

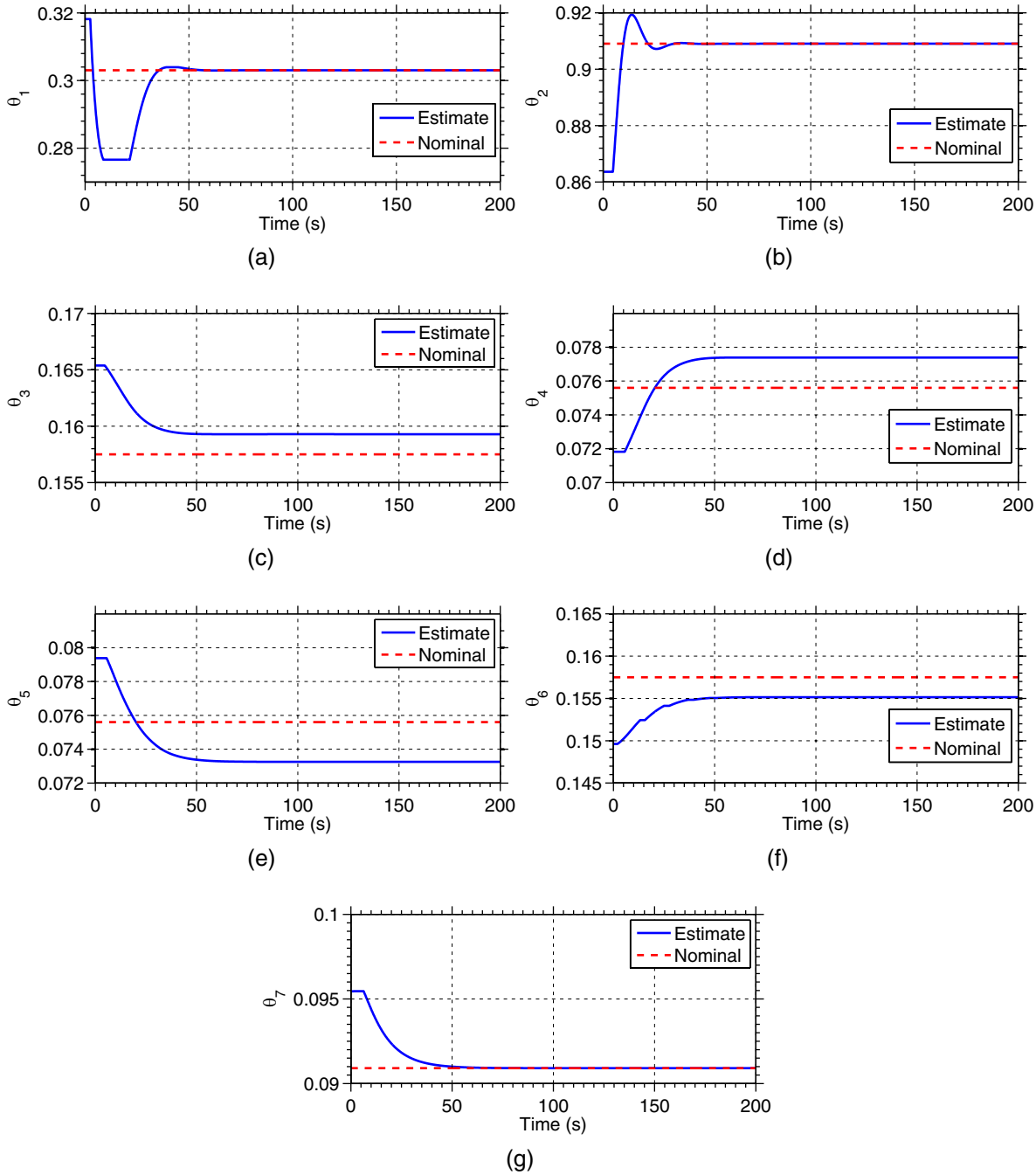

Figure 9. Comparison of estimated and nominal model parameters during the simulation of scenario 3 (constrained case).

select the free design parameters based on assessment of performance and robustness of the proposed scheme within a range of expected conditions and model parameters. Such a study will also be used to study the effect of different actuator constraints on the reachable operating space of the reactor. The robustness of the scheme will also be studied using predictive integrated modeling codes like METIS, CRONOS, or TRANSP, which include additional complexity, like actuator dynamics, evolving plasma geometry, and spatially varying temperature and density profiles. Additional actuation methods, including active pumping and modification of confinement properties through changes in magnetic parameters, will also be explored.

Acknowledgments

This work was supported by the NSF CAREER award program (ECCS-0645086) and the US Department of Energy (DEFG02-09ER55064, DE-FG02-92ER54141 and DE-FC02-04ER54698).

Appendix A. Particle recycling model derivation

The following particle recycling model derivation is based on a similar model derived in [33]. The particle balance for

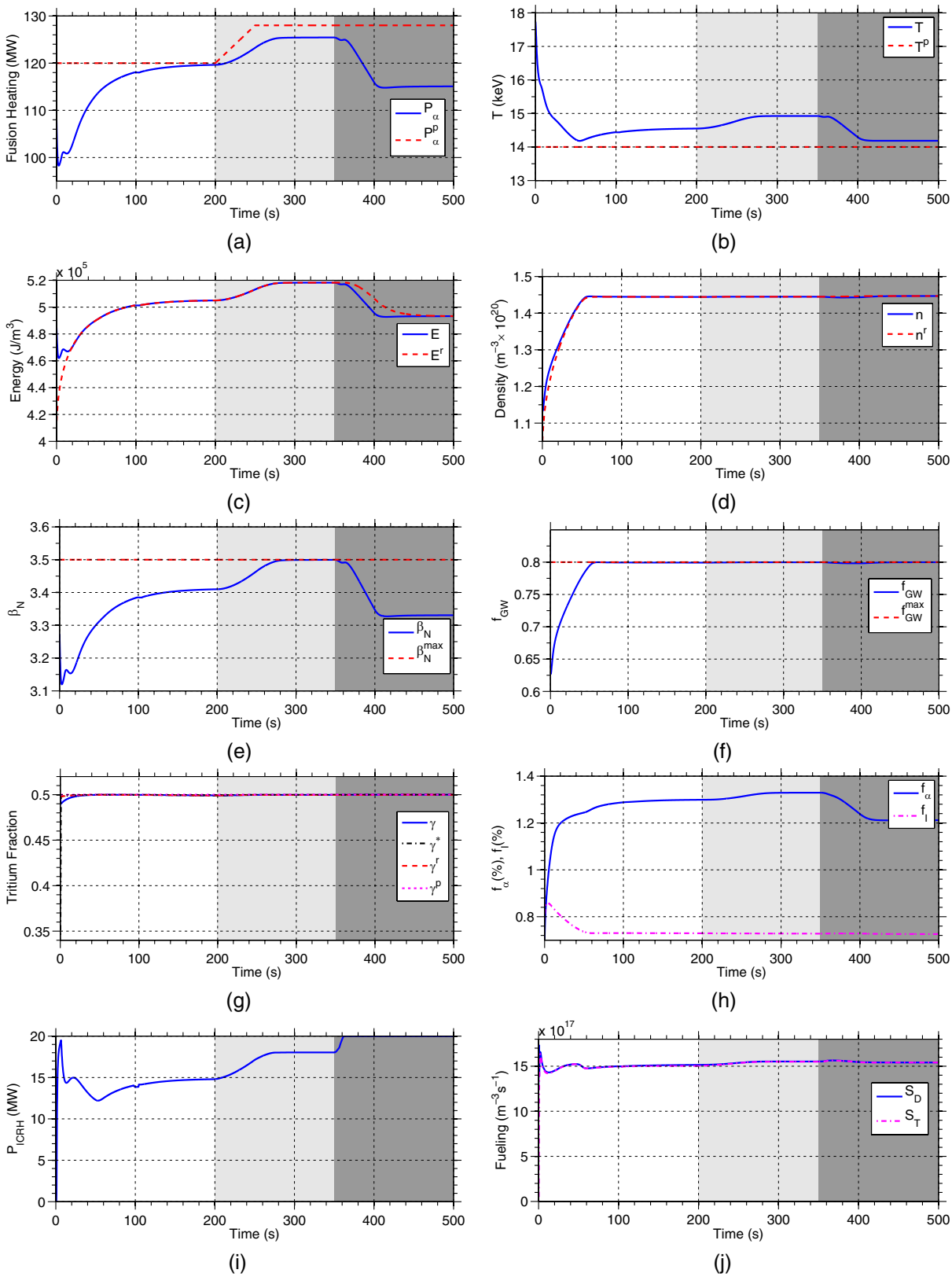

Figure 10. Closed loop evolution of (*a*) fusion heating, (*b*) temperature, (*c*) energy, (*d*) β_N, (*e*) f_{GW}, (*f*) density, (*g*) tritium fraction, (*h*) alpha-fraction and impurity fraction, along with (*i*) auxiliary heating and (*j*) fueling actuators during scenario 4.

deuterium and tritium ions can then be written as

$$\frac{dn_D}{dt} = -\frac{n_D}{\tau_D} + f_{eff} S_D^R + S_D^{inj}, \quad (A.1)$$

$$\frac{dn_T}{dt} = -\frac{n_T}{\tau_T} + f_{eff} S_T^R + S_T^{inj}, \quad (A.2)$$

where S_D^R and S_T^R represent the total recycling fluxes from the plasma facing components that reaches the plasma edge. The

recycled flux satisfies

$$S_{\mathrm{D}}^{\mathrm{R}} = f_{\mathrm{ref}} \frac{n_{\mathrm{D}}}{\tau_{\mathrm{D}}} + \left(1 - \gamma^{\mathrm{PFC}}\right) S^{\mathrm{PFC}} + f_{\mathrm{ref}} \left(1 - f_{\mathrm{eff}}\right) S_{\mathrm{D}}^{\mathrm{R}}, \quad \text{(A.3)}$$

$$S_{\mathrm{T}}^{\mathrm{R}} = f_{\mathrm{ref}} \frac{n_{\mathrm{T}}}{\tau_{\mathrm{T}}} + \gamma^{\mathrm{PFC}} S^{\mathrm{PFC}} + f_{\mathrm{ref}} \left(1 - f_{\mathrm{eff}}\right) S_{\mathrm{T}}^{\mathrm{R}}, \quad \text{(A.4)}$$

where γ^{PFC} is the tritium fraction of the particle flux from the plasma facing components, S^{PFC}. The third term in each expression represents the recycled flux that is screened by the plasma due to imperfect core fueling efficiency and subsequently reflected by the surface. We have not included screening of the fuel injection sources (S_D^{inj} and S_T^{inj}) to simplify presentation of the control design. Note that the terms neglected by this assumption could easily be handled by the proposed adaptive control approach in the same way as the remaining terms. To avoid the need for a self-consistent model of wall implantation, diffusion, and re-emission to obtain the desorbed flux S^{PFC}, we simplify the model by considering a recycling coefficient defined as the ratio of total recycling flux to the total flux to the surface, i.e.

$$R^{\mathrm{eff}} = \frac{S_{\mathrm{D}}^{\mathrm{R}} + S_{\mathrm{T}}^{\mathrm{R}}}{S_{\mathrm{D}}^{\mathrm{S}} + S_{\mathrm{T}}^{\mathrm{S}}} = \frac{S^{\mathrm{R}}}{S^{\mathrm{S}}}. \quad \text{(A.5)}$$

Note that the recycling coefficient includes the effect of wall pumping and active pumping. In order to incorporate the recycling coefficient into the model, we must write an expression for the flux to the surface

$$S_{\mathrm{D}}^{\mathrm{S}} = \frac{n_{\mathrm{D}}}{\tau_{\mathrm{D}}} + \left(1 - f_{\mathrm{eff}}\right)\left(1 - \gamma^{\mathrm{PFC}}\right) S^{\mathrm{PFC}} + f_{\mathrm{ref}} \left(1 - f_{\mathrm{eff}}\right) S_{\mathrm{D}}^{\mathrm{S}}, \quad \text{(A.6)}$$

$$S_{\mathrm{T}}^{\mathrm{S}} = \frac{n_{\mathrm{T}}}{\tau_{\mathrm{T}}} + \left(1 - f_{\mathrm{eff}}\right) \gamma^{\mathrm{PFC}} S^{\mathrm{PFC}} + f_{\mathrm{ref}} \left(1 - f_{\mathrm{eff}}\right) S_{\mathrm{T}}^{\mathrm{S}}, \quad \text{(A.7)}$$

where the third term represents the surface flux that is reflected and subsequently returned to the surface due to imperfect fueling efficiency. Since the recycling coefficient compares total hydrogen fluxes, not individual isotopes, we sum corresponding equations to obtain

$$S^{\mathrm{R}} = f_{\mathrm{ref}} \left(\frac{n_{\mathrm{D}}}{\tau_{\mathrm{D}}} + \frac{n_{\mathrm{T}}}{\tau_{\mathrm{T}}}\right) + S^{\mathrm{PFC}} + f_{\mathrm{ref}} \left(1 - f_{\mathrm{eff}}\right) S^{\mathrm{R}}, \quad \text{(A.8)}$$

$$S^{\mathrm{S}} = \frac{n_{\mathrm{D}}}{\tau_{\mathrm{D}}} + \frac{n_{\mathrm{T}}}{\tau_{\mathrm{T}}} + \left(1 - f_{\mathrm{eff}}\right) S^{\mathrm{PFC}} + f_{\mathrm{ref}} \left(1 - f_{\mathrm{eff}}\right) S^{\mathrm{S}}. \quad \text{(A.9)}$$

Using these expressions, we can solve to obtain

$$S^{\mathrm{PFC}} = S^{\mathrm{R}} \left[1 - f_{\mathrm{ref}} \left(1 - f_{\mathrm{eff}}\right)\right] - f_{\mathrm{ref}} \left(\frac{n_{\mathrm{D}}}{\tau_{\mathrm{D}}} + \frac{n_{\mathrm{T}}}{\tau_{\mathrm{T}}}\right), \quad \text{(A.10)}$$

$$S^{\mathrm{S}} = \left(\frac{n_{\mathrm{D}}}{\tau_{\mathrm{D}}} + \frac{n_{\mathrm{T}}}{\tau_{\mathrm{T}}}\right) + \left(1 - f_{\mathrm{eff}}\right) S^{\mathrm{R}}.$$

From the definition of the recycling coefficient, we have that $S^{\mathrm{S}} = S^{\mathrm{R}}/R^{\mathrm{eff}}$. Substituting this definition and rearranging, we can obtain

$$S^{\mathrm{R}} = \frac{R^{\mathrm{eff}}}{1 - R^{\mathrm{eff}} \left(1 - f_{\mathrm{eff}}\right)} \left(\frac{n_{\mathrm{D}}}{\tau_{\mathrm{D}}} + \frac{n_{\mathrm{T}}}{\tau_{\mathrm{T}}}\right). \quad \text{(A.11)}$$

Substituting into (A.10) yields

$$S^{\mathrm{PFC}} = \left[\frac{\left(1 - f_{\mathrm{ref}} \left(1 - f_{\mathrm{eff}}\right)\right) R^{\mathrm{eff}}}{1 - R^{\mathrm{eff}} \left(1 - f_{\mathrm{eff}}\right)} - f_{\mathrm{ref}}\right] \left(\frac{n_{\mathrm{D}}}{\tau_{\mathrm{D}}} + \frac{n_{\mathrm{T}}}{\tau_{\mathrm{T}}}\right). \quad \text{(A.12)}$$

Solving (A.3) and (A.4) for $S_{\mathrm{D}}^{\mathrm{R}}$ and $S_{\mathrm{T}}^{\mathrm{R}}$, respectively, and substituting (A.12) results in

$$S_{\mathrm{D}}^{\mathrm{R}} = \frac{1}{1 - f_{\mathrm{ref}} \left(1 - f_{\mathrm{eff}}\right)} \left\{ f_{\mathrm{ref}} \frac{n_{\mathrm{D}}}{\tau_{\mathrm{D}}} + \left(1 - \gamma^{\mathrm{PFC}}\right) \left[\frac{\left(1 - f_{\mathrm{ref}} \left(1 - f_{\mathrm{eff}}\right)\right) R^{\mathrm{eff}}}{1 - R^{\mathrm{eff}} \left(1 - f_{\mathrm{eff}}\right)} - f_{\mathrm{ref}}\right] \times \left(\frac{n_{\mathrm{D}}}{\tau_{\mathrm{D}}} + \frac{n_{\mathrm{T}}}{\tau_{\mathrm{T}}}\right) \right\}, \quad \text{(A.13)}$$

$$S_{\mathrm{T}}^{\mathrm{R}} = \frac{1}{1 - f_{\mathrm{ref}} \left(1 - f_{\mathrm{eff}}\right)} \left\{ f_{\mathrm{ref}} \frac{n_{\mathrm{T}}}{\tau_{\mathrm{T}}} + \gamma^{\mathrm{PFC}} \left[\frac{\left(1 - f_{\mathrm{ref}} \left(1 - f_{\mathrm{eff}}\right)\right) R^{\mathrm{eff}}}{1 - R^{\mathrm{eff}} \left(1 - f_{\mathrm{eff}}\right)} - f_{\mathrm{ref}}\right] \times \left(\frac{n_{\mathrm{D}}}{\tau_{\mathrm{D}}} + \frac{n_{\mathrm{T}}}{\tau_{\mathrm{T}}}\right) \right\}. \quad \text{(A.14)}$$

Appendix B. Optimization modification for $P_{\mathrm{ICRH}} = P_{\mathrm{ICRH}}^{\mathrm{max}}$ and $\gamma^* = 0.5$

Although the proposed optimization scheme can be programmed to respect a maximum heating power ($P_{\mathrm{ICRH}}^{\mathrm{max}}$ in the simulation study) in selecting the optimal operating point, it is possible that a selected feasible operating point may not be achievable from a particular initial state due to the nonlinear dependence of confinement and fusion power and the state. For example, an amount of heating exceeded the available power may initially be required to achieve a state for which fusion heating becomes large enough to sustain the operating point with only the available amount of heating power. Since the optimalvalues of n^r, γ^r, and E^r are interdependent, the values of n^r and γ^r will no longer be optimal of E^r is not achieved. To overcome this issue, the optimization scheme is augmented with an anti-windup-like logic: if the tritium fraction is at its maximum allowable value and $P_{\mathrm{aux}}^{\mathrm{unsat}} > P_{\mathrm{aux}}^{\mathrm{sat}}$, the energy reference is reduced until $P_{\mathrm{aux}}^{\mathrm{unsat}} = P_{\mathrm{aux}}^{\mathrm{sat}}$, i.e.,

$$\dot{E}^r = -k_{\mathrm{AW}} \left(P_{\mathrm{aux}}^{\mathrm{unsat}} - P_{\mathrm{aux}}^{\mathrm{sat}}\right), \quad \text{(B.1)}$$

where $k_{\mathrm{AW}} > 0$ is a free parameter. This ensures that E^r is driven to an achievable value for which the optimal values of n^r and γ^r can then be found.

References

[1] Mandrekas J and Stacey W M 1989 Evaluation of different burn control methods for the International Thermonuclear Experimental Reactor *Proc. 13th IEEE/NPSS Symp. Fusion Engineering (Knoxville, TN)* pp 404–7

[2] Haney S, Perkins L J, Mandrekas J and Stacey W M 1990 *Fusion Sci. Technol.* **18** 606

[3] Anderson D, Elevant T, Hamen H, Lisak M and Persson H 1993 *Fusion Sci. Technol.* **23** 5

[4] Bromberg L, Fisher J L and Cohn D R 1980 *Nucl. Fusion* **20** 203

[5] Chaniotakis E, Freidberg J and Cohn D 1990 CIT burn control using auxiliary power modulation *Proc. 13th IEEE/NPSS Symp. Fusion Engineering (Knoxville, TN)* pp 400–3

[6] Haney S and Perkins L 1990 Operating point selection, burn stability control for the International Thermonuclear Experimental Reactor *Proc. 13th IEEE/NPSS Symp. Fusion Engineering (Knoxville, TN)* pp 396–9

[7] Ashby D and Hughes M H 1980 *Nucl. Fusion* **20** 451
[8] Hui W and Miley G H 1992 *Bull. Am. Phys. Soc.* **37** 1399
[9] Bamieh B A, Hui W and Miley G H 1994 *Fusion Sci. Technol.* **25** 318
[10] Hui W, Fischbach K, Bamieh B A and Miley G H 1994 Effectiveness, constraints of using the refueling system to control fusion reactor burn *15th IEEE/NPSS Symp. Fusion Engineering (Hyannis, MA)* vol 2 pp 562–4
[11] Plummer D 1995 *Proc. 16th IEEE/NPSS Symp. Fusion Engineering on Fusion Reactor Control (Champaign, IL)* vol 2 pp 1186–9
[12] Mitarai O *et al* 2010 *Plasma Fusion Res.* **5** S1001
[13] Sestero A 1983 *Fusion Sci. Technol.* **4** 437
[14] Mitarai O and Muraoka K 1999 *Nucl. Fusion* **39** 725
[15] Sager G, Miley G and Maya I 1985 *Fusion Sci. Technol.* **8** 1795
[16] Mitarai O 2002 *Fuel Ratio, Fueling Control for Safe Ignited Operation in ITER class Tokamak Reactors* (*Advances in Plasma Physics Research* vol 2) (Hunlington, NY: Nova Science Publishers) p 37
[17] Firestone M A and Kessel C E 1991 *IEEE Trans. Plasma Sci.* **19** 29–41
[18] Miley G and Varadarajan V 1992 *Fusion Sci. Technol.* **22** 425
[19] Fuchs V, Shoucri M M, Thibaudeau G, Harten L and Bers A 1983 *IEEE Trans. Plasma Sci.* **PS-11** 4
[20] Leonov V M, Mitrishkin Y V and Zhogolev V E 2005 Simulation of burning ITER plasma in multi-variable kinetic control system *32nd EPS Conf. on Plasma Physics (Tarragona, Spain)* vol 29 pp 2–5
[21] Schuster E, Krstic M and Tynan G 2003 *Fusion Sci. Technol.* **43** 18
[22] Vitela J 2001 *Plasma Phys. Control. Fusion* **43** 99
[23] Vitela J 1998 *Plasma Phys. Control. Fusion* **40** 295
[24] Boyer M and Schuster E 2011 Zero-dimensional nonlinear burn control using isotopic fuel tailoring for thermal excursions *IEEE Conf. Control Applications* pp 246–51 (Piscataway, NJ: IEEE)
[25] Gouge M J, Houlberg W A, Attenberger S E and Milora S L 1995 *Fusion Sci. Technol.* **4** 1644–50
[26] Baylor L *et al* 2007 *Nucl. Fusion* **47** 443
[27] Asai K *et al* 2006 *J. Nucl. Sci. Technol.* **43** 320
[28] Okada K *et al* 2007 *Plasma Fusion Res.* **2** S1083
[29] Adetola V and Guay M 2006 *J. Process Control* **16** 521
[30] Guay M and Zhang T 2003 *Automatica* **39** 1283
[31] Hively L 1977 *Nucl. Fusion* **17** 873
[32] Andrew P *et al* 1999 *J. Nucl. Mater.* **266–269** 153
[33] Ehrenberg J 1996 Wall effects on particle recycling in tokamaks *Physical Processes of the Interaction of Fusion Plasmas with Solids* (New York: Academic) p 35
[34] Stacey W M 2010 *Fusion: An Introduction to the Physics, Technology of Magnetic Confinement Fusion* 2nd edn (Weinheim: Wiley-VCH)
[35] 2001 Summary of the ITER final design report *Technical Report* International Atomic Energy Agency, Vienna
[36] Byrd R H, Hribar M E and Nocedal J 1999 *SIAM J. Optim.* **9** 877
[37] Byrd R H, Gilbert J C and Nocedal J 2000 *Math. Programming* **89** 149
[38] Khalil H K 2002 *Nonlinear Systems* 3rd edn (Englewood Cliffs, NJ: Prentice Hall)
[39] Krstić M, Kanellakopoulos I and Kokotović P 1995 *Nonlinear, Adaptive Control Design* (New York: Wiley)
[40] Adetola V and Guay M 2006 *J. Process Control* **16** 521–33
[41] Boyer M and Schuster E 2014 Nonlinear burn control in tokamak fusion reactors via output feedback *Proc. 19th World Congress of the International Federation of Automatic Control (Cape Town, South Africa)* accepted